DEPARTMENT OF PHYSICS, UNIVERSITY OF JYVÄSKYLÄ
RESEARCH REPORT No. 5/2000

PHASES AND PHASE TRANSITIONS IN RESTRICTED SYSTEMS

BY
DRAGOŞ-VICTOR ANGHEL

Academic Dissertation
for the Degree of
Doctor of Philosophy

Jyväskylä, Finland
May 2000

URN:ISBN:978-951-39-9456-3
ISBN 978-951-39-9456-3 (PDF)
ISSN 0075-465X

Jyväskylän yliopisto, 2022

ISBN 951-39-0707-4
ISSN 0075-465X

DEPARTMENT OF PHYSICS, UNIVERSITY OF JYVÄSKYLÄ
RESEARCH REPORT No. 5/2[redacted]

PHASES AND PHASE TRANSITIONS IN RESTRICTED SYSTEMS

BY
DRAGOŞ-VICTOR ANGHEL

Academic Dissertation
for the Degree of
Doctor of Philosophy

To be presented, by permission of the
Faculty of Mathematics and Natural Sciences
of the University of Jyväskylä,
for public examination in Auditorium FYS-1 of the
University of Jyväskylä on May 26, 2[redacted]
at 12 o'clock noon

Jyväskylä, Finland
May 2[redacted]

Preface

The work reviewed in this thesis has been carried out during the years 1997–1999 at the Department of Physics in the University of Jyväskylä.

I want to thank my supervisor, Prof. Matti Manninen, for his excellent and inspiring guidance in physics in particular, and in research work in general. It was also a great opportunity and challenge to work with Prof. Jukka Pekola. He brought to my attention delightful problems that showed up in the experiments done in his group. Most of my work is either based on, or inspired by these problems. He helped me understand many aspects of both theoretical and experimental physics. Working with Professors Matti Manninen and Jukka Pekola was very pleasant.

Thanks are due to Dr. Anniina Rytkönen and Dr. Hannu Häkkinen for many discussions about cluster physics. Dr. Anniina Rytkönen kindly provided me the FORTRAN codes for the Molecular Dynamics simulations of Publication V. Prof. Jussi Timonen and Dr. Juha Merikoski are gratefully acknowledged for many useful discussions related to statistical mechanics and mathematical physics. I want to thank Dr. Konstantin Arutyunov, Dr. P. S. Deo, Prof. F. M. Peeters, Dr. Roberto Leoni, Dr. Joel Ullom, Prof. B. J. van Wees, Prof. A. G. Kozorezov, and Mr. Jochem Baselmans for discussions about Publication IV.

Warm thanks are due to the staff of the Department of Physics for a lot of help with all the practical problems and for providing a nice working atmosphere.

The financial support from the Center for International Mobility, the Graduate School of Material Physics, the Academy of Finland, the Nyyssönen Foundation, and the travel founds from the Soros Foundation are gratefully acknowledged.

Most of all I want to thank my beloved wife Anamirela and my sweet little daughter Maria for all the joy and happiness they bring into my life, and for their continuous encouragement. This thesis, together with all my work, is dedicated to them.

Jyväskylä, May 2000

Dragoş-Victor Anghel

Abstract

This thesis is a review of five publications in which some effects characteristic to systems with restricted dimensions are emphasised. These effects are *the Bose-like condensation*, *the divergency of the specific heat at zero temperature in Fermi systems*, *the diffusion of nonequilibrium quasiparticles in mesoscopic superconductors*, and the existence of the *core-melted cluster*.

The first of these effects, the Bose-like condensation, arises from the freezing out of one or more degrees of freedom of particles in a mesoscopic system. During this process, the dimensionality of the particle distribution is changing and analogies can be made with the multiple-step Bose-Einstein condensation. The Bose-like condensation was first observed in the phonon gas inside an ultrathin dielectric membrane at low temperatures. Nevertheless, it can be extended to systems of massive particles and it occurs for both bosons and fermions.

In the case of fermions, for certain types of single particle hamiltonians, the specific heat has asymptotically a divergent behavior at zero temperature, as the Fermi energy $\epsilon_{\rm F}$ approaches any value from an infinite discrete set of energies: $\{\epsilon_i\}_{i\geq 1}$. The divergent behavior for $\epsilon_{\rm F} = \epsilon_i$, for any i, is specific to infinite systems. If the system is finite, the specific heat converges to zero at zero temperature, for any $\epsilon_{\rm F}$, as expected. All the results are particularized for particles trapped inside parallelepipedic boxes and harmonic potentials.

The diffusion of nonequilibrium quasiparticles injected into mesoscopic superconducting wires was analyzed in connection with the cooling properties of normal metal–insulator–superconductor tunnel junctions. It turns out that due to the superconducting energy gap, the diffusion in bare superconducting wires is poor, but it can be very much enhanced by depositing a normal metal film in contact with this nano-sized wire. If there is an insulating oxide layer between the normal metal and the superconductor, the quasiparticles from the superconductor can tunnel into the normal metal, reducing in this way the electronic temperature of the superconductor. If the normal metal is in good metal-to-metal contact with the superconductor, the spatial variation of the energy gap strongly enhances the quasiparticle current.

Finally, the possibility of the existence of a core-melted cluster was investigated. A pair potential was introduced, with the property that the solid state of the cluster is less dense than the liquid state. With this kind of potential the cluster exhibits quite an unusual behavior. In addition to the known states, solid, liquid and surface-melted, it can also be found in a “dense liquid” phase (a disordered state appearing at low temperatures), a “core-melted” phase and a “core-surface-melted” phase. In the core-melted phase the external part of the cluster consists

of atoms that vibrate around regular crystalline sites, while the core atoms have much bigger mobility and sometimes exhibit diffusive motion.

List of publications

I **Properties of the Phonon Gas in Ultrathin Membranes at Low Temperature**
D. V. Anghel, J. P. Pekola, M. M. Leivo, J. K. Suoknuuti, and M. Manninen
Phys. Rev. Lett. **81**, 2958 (1998).
https://doi.org/10.1103/PhysRevLett.81.2958

II **Behaviour of the Phonon Gas in restricted geometries**
D. V. Anghel and M. Manninen
Phys. Rev. **B59**, 9854 (1999).
https://doi.org/10.1103/PhysRevB.59.9854

III **Dimensionality effects in restricted bosonic and fermionic systems**
D. V. Anghel
Submitted to Phys. Rev. E.
https://doi.org/10.1103/PhysRevE.62.7658

IV **Trapping of quasiparticles of a non-equilibrium superconductor**
J.P. Pekola, D.V. Anghel, T.I. Suppula, J.K. Suoknuuti, A.J. Manninen, and M. Manninen
Appl. Phys. Lett. **76**, 2782 (2000).
https://doi.org/10.1063/1.126474

V **Core-melted clusters**
D. V. Anghel and M. Manninen
Eur. Phys. J. D **9**, 437 (1999).
https://doi.org/10.1007/978-3-642-88188-6_87

All the new models and theoretical innovations introduced in the papers above are the creation of the author of this thesis. He also performed all the analytical and numerical calculations and had a central role in interpreting the results. The computer codes needed in the calculations and in fitting and sorting the data, were also written by the author. The only exception was the Molecular Dynamics code used for the simulations in paper **V**, which was kindly provided by Dr. A. Rytkönen. Here the author modified the code for this specific problem. Neither did he take part in any of the experiments.

The author of this thesis wrote the papers **II**, **III**, and **V**, most of the paper **I**, and the theory part of paper **IV**.

Erratum

There are some mistakes in Publication I. Equation (10) is printed incorrectly. The correct form is

$$
\begin{aligned}
p_\kappa &= (2-l) + \\
&\left\{ \sum_{n=1}^{\infty} \int_{nx_0}^{\infty} \mathrm{d}x \frac{2(nx_0)^2 x^{1-l} + C_s C_l \left(\frac{k_B T}{\hbar v_s}\right)^{2-l} \frac{(nx_0)x^{2-2l}}{l_3} ((nx_0)^2 + x^2)}{\left[1 + C_s C_l \left(\frac{k_B T}{\hbar v_s}\right)^{2-l} \frac{(nx_0)x^{1-l}}{l_3}\right]^2} \right. \\
&\left. \times \frac{e^x}{(e^x - 1)^2} \right\} \\
&\times \left\{ \sum_{n=0}^{\infty} \int_{nx_0}^{\infty} \mathrm{d}x \frac{x^{1-l}(x^2 - (nx_0)^2)}{1 + C_s C_l \left(\frac{k_B T}{\hbar v_s}\right)^{2-l} \frac{(nx_0)x^{1-l}}{l_3}} \frac{e^x}{(e^x - 1)^2} \right\}^{-1} .
\end{aligned}
$$

Also, on the first page, second paragraph, it is written

$$\omega_{3_{min}} = v_s \times (2\pi/l_3) \approx 1.1 \times 10^{11} \ \mathrm{s}^{-1},$$

while the correct form is

$$\omega_{3_{min}} = v_s \times (\pi/l_3) \approx 1.1 \times 10^{11} \ \mathrm{s}^{-1}.$$

The inset of Fig. 2 is wrong (the main frame is correct). The correct figure is shown on the next page. Moreover, the expression *specific heat* was used instead of *heat capacity* and the Bose-Einstein condensation was called a phase transition of *order two*, while in reality it is of *order one*.

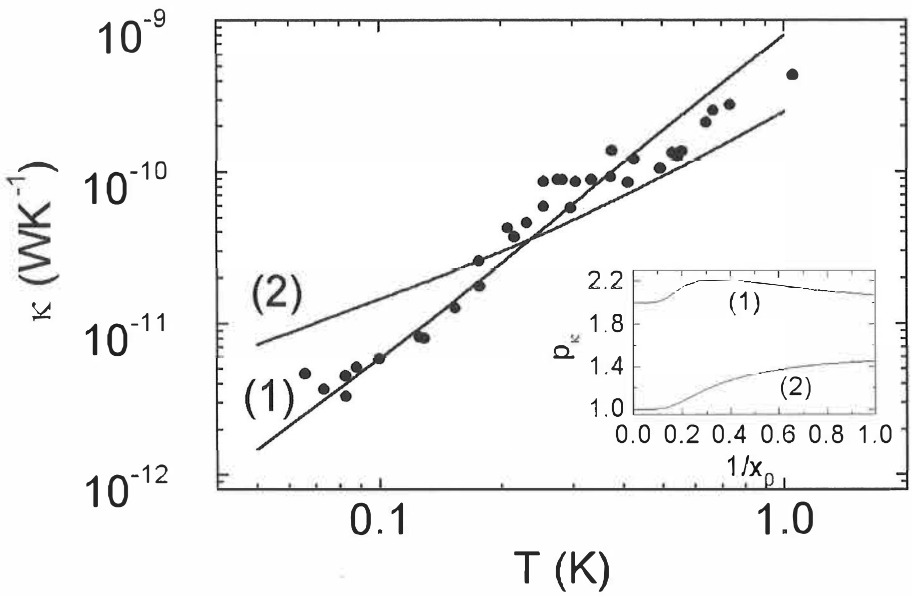

Figure 2: The experimental data (the dots) and the theoretical curves (9) for curve (1): $l = 0$ and $C_l \approx 10.3 \times 10^{-6}$ (m); curve (2): $l = 1$ and $C_l \approx 101.9$. We used $v_s = 7200$ ms^{-1}, $l_3 = 200$ nm and $C_s \approx 5 \times 10^{-17}$ m^2. The inset shows the exponents of the temperature dependence of κ [Eq. (10)] corresponding to the curves (1) and (2) in the main figure.

Contents

Chapter 1

Classification of phases and phase transitions in statistical mechanics

1.1 Introduction

The world around us can be divided into physical systems in interaction with each other. Each of these systems consists of substances in different phases. Some of these, like the solid, liquid, and gaseous phases, or even the different magnetization states, are easy to observe even for a nonspecialist. Others, like the superconducting phase, the Bose-condensed phases, the regularity and symmetry of the crystalline lattice, and the phases of mesoscopic objects or clusters, require special experimental devices to be produced and identified. Understanding the phases and the transitions between them is an important part of understanding the nature. Yet, despite all the theoretical and experimental efforts in this direction, there are still many open questions.

There is a great variety of models, some of which are exactly solvable, that can explain quantitatively or qualitatively many properties of matter. For example, one can use a model based on *ideal noninteracting particles*, described in almost any textbook of statistical mechanics (see Ref. [1]), to explain to some extent the properties of gases, the Bose-Einstein condensation of low density particles inside different kinds of traps, and even some of the properties of electrons inside conductors or semiconductors, or thermal properties of dielectrics. To improve beyond the results obtained using the ideal gas, a *mean field method* can be employed [2]. With this method one can make calculations for systems at higher particle densities. Besides this, properties that could not be described by the ideal gas, like, for example, the magnetic properties, are tractable using the mean field method. More sophisticated techniques, like perturbation theory applied to classical or quantum statistical mechanics [1], or to quantum field theory [3], can be used to describe more complicated systems or special properties.

However, in all the systems, the phase transitions are among the most difficult phenomena to describe, using a microscopical model. A special case constitutes the first order phase transitions between solid, liquid and gaseous phases, since, using approximative methods for calculations, one cannot obtain jumps in the first order derivatives of the Gibbs potential. Fortunately a set of theorems introduced by Yang and Lee [4] clear the way by showing that, for example in a gas with a realistic interaction among particles, a discontinuous first order phase transition can occur, as expected in real gases.

In the next section I shall discuss shortly the classification of phase transitions in thermodynamics. The phases and the phase transitions are rigorously defined in bulk systems. In finite systems of small dimensions (mesoscopic systems) the differences between phases are smeared out and sometimes it becomes a matter of convenience how one can define the phases and the border between them, in the parametric space. These aspects will be discussed in section 1.3. In clusters the situation is even more complicated, since they can transform competely from one phase to another. The phases can be defined with difficulty, maybe with very few exceptions, like, for example, the solid phase at a very low temperature. This is the reason why it is more appropriate to discuss *phase-like forms* instead of phases in this situation. We say that a cluster is in a certain phase-like form when it exhibits most of the properties of that specific phase, as defined in bulk systems [5]. The phase-like forms of clusters will be discussed in general in section 1.4. In the remaining chapters I shall present briefly my own contribution to these subjects.

1.2 Bulk systems

Strictly speaking, thermodynamics is defined only for bulk systems. Formally this corresponds to the assumption that the number of particles and the volume of the system under investigation are enormous, at a finite particle density. From a practical point of view, the bulk systems are those in which the relative fluctuations of all the thermodynamical quantities are negligible. In all this section I shall refer only to this kind of systems.

1.2.1 First order phase transitions

In bulk systems the phases are well defined and, by definition, there are no fluctuations that would bring the systems from one phase to another. The phase transition can be identified by a discontinuity in the thermodynamic potential describing the system, or in its derivatives. For example, to describe the first order phase transition from gas to liquid or vice versa, the Gibbs function is the appropriate thermodynamical potential. The Gibbs function per mole is the chemical potential, and its derivatives are the molar volume and the molar entropy. At the phase transition, these last two quantities are discontinuous. The jump in entropy is related to the latent heat and the change in volume is due to the different densities of the two phases. A schematic curve corresponding to a phase transition in PT coordinates (pressure vs. temperature) is shown in Fig. 1.1. The line separating the two phases ends at the critical point. The existence of the critical point is a characteristic of the phase transition of order one. Due to this property, a system can be brought from one phase into another by encircling the critical point, hence without experiencing any phase transition.[1] The slope

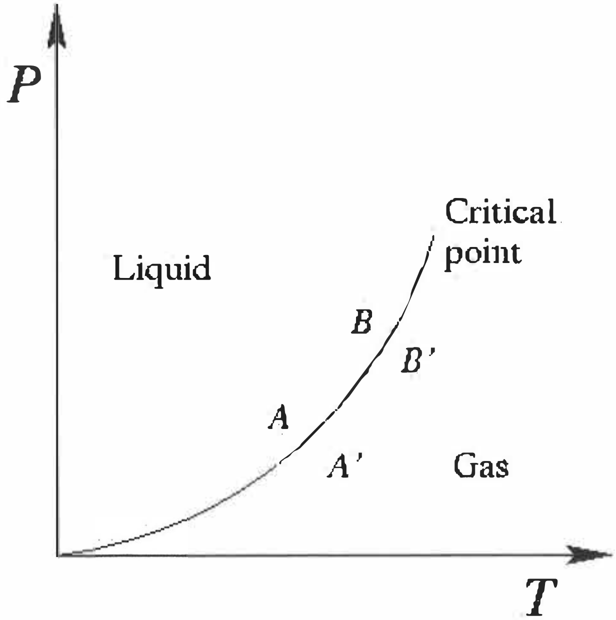

Figure 1.1: The curve corresponding to the transition between liquid and gas phases of a neutral fluid. The transition is of order one and the natural thermodynamic potential, the Gibbs function, depends just on pressure P and temperature T at constant particle number.

of the separation line between the phases is related to the jumps in the molar entropy and the molar volume by the *Clapeyron-Clausius equation*. To derive this we choose four points A, B, A', and B', as shown in Fig. 1.1. The points A and B are, in the limit, on the border of the liquid phase, while A' and B' are on the same border, in the same positions as A and B, respectively, but seen as

[1]Nevertheless, one should keep in mind the Bose-Einstein condensation of ideal bosons as an example of a first order phase transition that does not have a critical point. In this case, for a three dimensional gas inside a box with impenetrable walls, the phase equilibrium curve extends towards the point ($P = \infty, T = \infty$) along a curve $P \propto T^{5/2}$ [6].

belonging to the gaseous phase. The continuity of the thermodynamical potential at the phase transition implies that

$$\mu_A = \mu_{A'} \,, \tag{1.1}$$

and

$$\mu_B = \mu_{B'} \,. \tag{1.2}$$

Using the differential equations

$$d\mu = -sdT + vdP \tag{1.3}$$

and

$$d\mu' = -s'dT + v'dP \tag{1.4}$$

corresponding to the liquid and gas phases respectively, we obtain the result

$$\frac{dP}{dT} = \frac{\Delta s}{\Delta v} = \frac{l}{T\Delta v}, \tag{1.5}$$

where $\Delta s = s' - s$ and $\Delta v = v' - v$, while l is the latent heat. The molar entropies and volumes in the two phases are denoted by s, s' and v, v', respectively. An equation of the form (1.5) can be written for any first order phase transition (like liquid-solid, solid-gas, etc.), not only for the transition between liquid and gas.

Since it will be of interest in the subsequent chapters, some of the properties of the ideal Bose gases will be outlined here. It is already well known that a d dimensional Bose gas inside a cuboidal box, experiences a first order phase transition, the so called *Bose condensation*, as the particle density is increased at constant temperature, or as the temperature is decreased at constant density, for $d \geq 3$. At the transition temperature, T_c (constant density), the ground state of the system becomes macroscopically occupied. At this point, in the limit $V \to \infty$, the chemical potential converges to zero and the specific heat exhibits a cusp-like maximum for $d = 3, 4$ and a discontinuity for $d \geq 5$, as shown in Fig. 1.2 [6]. The transition temperature is defined by the relation

$$\lambda_\mathrm{c}^d = \zeta(d/2)/\rho, \tag{1.6}$$

where $\lambda_\mathrm{c} = \sqrt{h^2/(2\pi m k_\mathrm{B} T_\mathrm{c})}$ is the thermal wavelength corresponding to the transition temperature T_c, $\zeta(x)$ is the Riemann zeta function of argument x, ρ is the d-dimensional particle density, and m is the particle mass.

If the dimensionality of the Bose gas is two or one, there is no Bose condensation in cuboidal boxes. In this case we can define a scaling temperature by the formula

$$\lambda_\mathrm{s}^d = 1/\rho, \tag{1.7}$$

where $\lambda_\mathrm{s} = \sqrt{h^2/(2\pi m k_\mathrm{B} T_\mathrm{s})}$. In Fig. 1.2 we present the specific heat per particle, as a function of the scaled temperature, for the cases discussed.

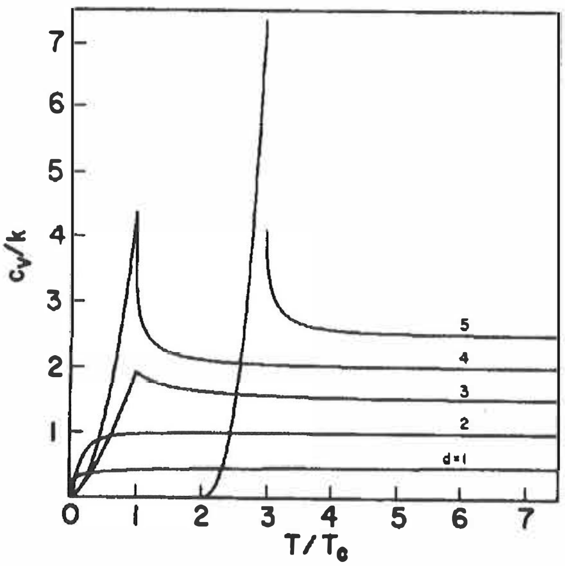

Figure 1.2: The specific heat per particle, as a function of the scaled temperature, for Bose gases of dimension $d = 1$ to 5 in cuboidal boxes. In the case $d = 5$ the curve is displaced by two units along the horizontal axis. Taken from R.M. Ziff, G.E. Uhlenbeck, and M. Kac, Phys. Rep. **32**, 169 (1977).

The Bose condensation has also been discussed for particles in different kinds of traps and in different dimensions (see, for example, [7, 8] for power-law traps). The observation of the phenomenon in systems of atoms trapped in magnetic field [9] motivated the theoretical investigation of the Bose condensation in harmonic traps. A three dimensional (3D) distribution of bosons in such a trap experiences a Bose condensation at the temperature $T_{\mathrm{c,h}} \equiv (\hbar/k_{\mathrm{B}})[N\omega_1\omega_2\omega_3]/\zeta(3)]^{1/3}$, where $\omega_{1,2,3}$ are the frequencies of the harmonic potential in the directions x, y, and z, and N is the number of particles. When $N \to \infty$ and $N\omega_1\omega_2\omega_3$ is finite, the transition is abrupt and the specific heat has a discontinuity at the transition temperature [7, 10].

1.2.2 Higher order phase transitions

For higher order phase transitions the molar parameters are continuous, but some of their higher order derivatives are discontinuous. There are two classifications of these phase transitions. The first and simplest one is due to Ehrenfest. In this classification a phase transition is of order n if all the derivatives of order less than n are continuous while the ones of order n have jumps at the phase transition. In this case, equations similar to the *Clapeyron-Clausius equation* can be written for the jumps in the discontinuous quantities when passing from one phase into the other. These equations are known as Ehrenfest's equations (see, for example [2]). For example the derivative of the pressure with respect to the temperature along the curve separating the phases, in the case of a second order phase transition, is related to the jumps in the specific heat, c_P, and the thermal expansion coefficient, $\varpi = (1/v)(\partial v/\partial T)_P$, at constant pressure by the relation:

$$\frac{dP}{dT} = \frac{1}{vT}\frac{\Delta c_P}{\Delta \varpi}. \tag{1.8}$$

The only real phase transition of order higher than one, in which the jumps of the thermodynamic parameters are finite, is the superconducting phase transition in zero magnetic field. The onset of the superconductivity is due to the attractive interaction between electrons, mediated by phonons [11]. This interaction binds electrons into pairs (Cooper pairs) which, in the simplest case, have total spin, momentum, and angular momentum equal to zero (s-wave). If the interacting electrons are situated above the filled Fermi sea, the wavefunction of their coupled state can be written in the form

$$\psi_0(\mathbf{r_1} - \mathbf{r_2}) = \left[\sum_{k>k_\mathrm{F}} g_\mathbf{k} \cos \mathbf{k}(\mathbf{r_1} - \mathbf{r_2})\right] (|\uparrow\rangle_1 |\downarrow\rangle_2 - |\downarrow\rangle_1 |\uparrow\rangle_2), \tag{1.9}$$

where the summation is over wave vectors $\mathbf{k}$ above the Fermi surface. The spin states of the electrons were denoted by $|\downarrow\rangle_{1,2}$ or $|\uparrow\rangle_{1,2}$. The constants $g_\mathbf{k}$ are nothing else but the coefficients of the expansion of the function $\psi_0(\mathbf{r_1} - \mathbf{r_2})$ in terms of the eigenvectors of the bare (renormalised) hamiltonian H_0. If we add the interaction V into the Schrödinger equation and solve it, using the simplifying assumption that $V_{\mathbf{k},\mathbf{k}'} = -V$ $(V > 0)$ if the bare energies $\epsilon_\mathbf{k}$ and $\epsilon_{\mathbf{k}'}$, are in the interval $(\epsilon_\mathrm{F}, \epsilon_\mathrm{F} + \hbar\omega_\mathrm{c})$ and zero otherwise [$V_{\mathbf{k},\mathbf{k}'}$ is the matrix element of the interaction operator $\hat{V}$ between the pairs of electrons $(\mathbf{k}, -\mathbf{k})$ and $(\mathbf{k}', -\mathbf{k}')$], we end up with an equation for the energy E of the Cooper pair:

$$\frac{1}{V} = \sum_{\substack{k \\ \epsilon_\mathbf{k} \in (\epsilon_\mathrm{F}, \epsilon_\mathrm{F} + \hbar\omega_\mathrm{c})}} (2\epsilon_\mathbf{k} - E)^{-1}. \tag{1.10}$$

If we transform the summation into an integral, with $N(0)$ the density of electron states at the Fermi energy, and assuming that $\hbar\omega_\mathrm{c} \ll \epsilon_\mathrm{F}$, we obtain

$$\frac{1}{V} = \frac{1}{2}N(0) \ln \frac{2\epsilon_\mathrm{F} - E + 2\hbar\omega_\mathrm{c}}{2\epsilon_\mathrm{F} - E}. \tag{1.11}$$

Since usually $N(0)V < 0.3$, we assume $N(0)V \ll 1$, and we can approximate the equation above by

$$E \approx 2\epsilon_\mathrm{F} - 2\hbar\omega_\mathrm{c} e^{-2/N(0)V}. \tag{1.12}$$

This is the so called *weak-coupling approximation.* We now observe that the state built up from electrons with $k > k_{\rm F}$ has an energy lower than the Fermi energy. Therefore, by decreasing the energy of the electrons close to the Fermi surface, this mechanism could eventually lead to the formation of a gap in the spectrum of the electrons, around this energy.

To evaluate the ground state of the interacting system, we have to use the formalism of the second quantization. For this we write the hamiltonian, $\hat{H}$, and the ground state of the system, $|BCS\rangle$, as

$$\hat{H} = \sum_{\mathbf{k},\sigma} \epsilon_{\mathbf{k}} c^+_{\mathbf{k}\sigma} c_{\mathbf{k}\sigma} + \sum_{\mathbf{k},\mathbf{l}} V_{\mathbf{k},\mathbf{l}} c^+_{\mathbf{k}\uparrow} c^+_{-\mathbf{k}\downarrow} c_{-\mathbf{l}\downarrow} c_{\mathbf{l}\uparrow} \tag{1.13}$$

and

$$|BCS\rangle = \prod_{\mathbf{k}=\mathbf{k}_1,\ldots,\mathbf{k}_{\rm M}} (u_{\mathbf{k}} + v_{\mathbf{k}} c^+_{\mathbf{k}\uparrow} c^+_{-\mathbf{k}\downarrow})|0\rangle, \tag{1.14}$$

respectively, where $|0\rangle$ is the vacuum state (no particles), and $\mathbf{k}_1$ ($\mathbf{k}_{\rm M}$) is the first (last) value that the wave number assumes in the band. For normalization reasons, $|u_{\mathbf{k}}|^2 + |v_{\mathbf{k}}|^2 = 1$. The average number of electrons in the system can be evaluated by calculating the matrix element of the particle number operator $\hat{N} = \sum_{\mathbf{k},\sigma} c^+_{\mathbf{k}\sigma} c_{\mathbf{k}\sigma}$ onto $|BCS\rangle$. The result is

$$\bar{N} = \sum_{\mathbf{k}} 2|v_{\mathbf{k}}|^2. \tag{1.15}$$

The probability of finding N particles in the system is sharply peaked around the value $\bar{N}$.

We now fix the average number of particles in the ground state by introducing the chemical potential μ. The ground state is found by minimizing the expectation value of the sum

$$\delta\langle BCS|\hat{H} - \mu\hat{N}|BCS\rangle = 0. \tag{1.16}$$

If we define the quantities:

$$\begin{aligned}
\xi_{\mathbf{k}} &= \epsilon_{\mathbf{k}} - \mu, \\
u_{\mathbf{k}} &= \sin\theta_{\mathbf{k}}, \\
v_{\mathbf{k}} &= \cos\theta_{\mathbf{k}}, \\
\Delta_{\mathbf{k}} &= -\textstyle\sum_{\mathbf{l}} V_{\mathbf{k},\mathbf{l}} u_{\mathbf{l}} v_{\mathbf{l}} = -\frac{1}{2}\sum_{\mathbf{l}} V_{\mathbf{k},\mathbf{l}} \sin 2\theta_{\mathbf{l}}, \\
E_{\mathbf{k}} &= (\Delta^2_{\mathbf{k}} + \xi^2_{\mathbf{k}})^{1/2},
\end{aligned} \tag{1.17}$$

and make use of Eq. (1.16), we obtain the following equations between the parameters:

$$\begin{aligned}
\tan 2\theta_{\mathbf{k}} &= -\tfrac{\Delta_{\mathbf{k}}}{\xi_{\mathbf{k}}}, \\
2u_{\mathbf{k}}v_{\mathbf{k}} &= \sin 2\theta_{\mathbf{k}} = \tfrac{\Delta_{\mathbf{k}}}{E_{\mathbf{k}}}, \\
\text{and} \qquad v^2_{\mathbf{k}} - u^2_{\mathbf{k}} &= \cos 2\theta_{\mathbf{k}} = -\tfrac{\xi_{\mathbf{k}}}{E_{\mathbf{k}}}.
\end{aligned} \tag{1.18}$$

Using again the assumption that

$$V_{\mathbf{k},\mathbf{l}} = \begin{cases} -V & \text{if } |\xi_{\mathbf{k}}| \text{ and } |\xi_{\mathbf{l}}| \leq \hbar\omega_{\mathrm{c}} \\ 0 & \text{otherwise} \end{cases}$$

and combining Eqs. (1.18) with (1.17) we obtain

$$\Delta_{\mathbf{k}} = \begin{cases} \Delta & \text{for } |\xi_{\mathbf{k}}| \leq \hbar\omega_{\mathrm{c}} \\ 0 & \text{otherwise} \end{cases},$$

with

$$\Delta = \frac{\hbar\omega_{\mathrm{c}}}{\sinh\left[1/N(0)V\right]} \approx 2\hbar\omega_{\mathrm{c}} e^{-1/N(0)V}. \tag{1.19}$$

The fractional occupation number $v_{\mathbf{k}}^2$ is given by

$$v_{\mathbf{k}}^2 = \frac{1}{2}\left[1 - \frac{\xi_{\mathbf{k}}}{(\Delta^2 + \xi_{\mathbf{k}}^2)^{1/2}}\right] \tag{1.20}$$

and

$$u_{\mathbf{k}}^2 = 1 - v_{\mathbf{k}}^2. \tag{1.21}$$

The energy difference between the normal and the superconducting ground states is equal to

$$\langle E\rangle_{\mathrm{n}} - \langle E\rangle_{\mathrm{s}} = \frac{1}{2}N(0)\Delta^2, \tag{1.22}$$

which is the condensation energy at zero temperature, in the absence of magnetic field.

The method outlined above is quite difficult to use at finite temperatures, since the excitations are difficult to handle. In what follows I shall present very briefly a self consistent field method, which is much more convenient for calculations.

We begin by formally defining the product of operators

$$c_{-\mathbf{k}\downarrow}c_{\mathbf{k}\uparrow} = b_{\mathbf{k}} + (c_{-\mathbf{k}\downarrow}c_{\mathbf{k}\uparrow} - b_{\mathbf{k}}),$$

in which $b_{\mathbf{k}}$ is interpreted as the average

$$b_{\mathbf{k}} = \langle c_{-\mathbf{k}\downarrow}c_{\mathbf{k}\uparrow}\rangle_{\mathrm{av}}.$$

If we redefine

$$\Delta_{\mathbf{k}} = -\sum_{\mathbf{l}} V_{\mathbf{k},\mathbf{l}} b_l = -\sum_{\mathbf{l}} V_{\mathbf{k},\mathbf{l}}\langle c_{-\mathbf{l}\downarrow}c_{\mathbf{l}\uparrow}\rangle_{\mathrm{av}}$$

and neglect the (presumably) small terms proportional to $(c_{-\mathbf{k}\downarrow}c_{\mathbf{k}\uparrow} - b_{\mathbf{k}})^2$, we can write the hamiltonian in a quadratic form:

$$H_M = \sum_{\mathbf{k},\sigma} \epsilon_{\mathbf{k}} c_{\mathbf{k}\sigma}^+ c_{\mathbf{k}\sigma} - \sum \mathbf{k}(\Delta_{\mathbf{k}} c_{\mathbf{k}\uparrow}^+ c_{-\mathbf{k}\downarrow}^+ + \Delta_{\mathbf{k}}^* c_{-\mathbf{k}\downarrow}c_{\mathbf{k}\uparrow} - \Delta_{\mathbf{k}} b_{\mathbf{k}}^*), \tag{1.23}$$

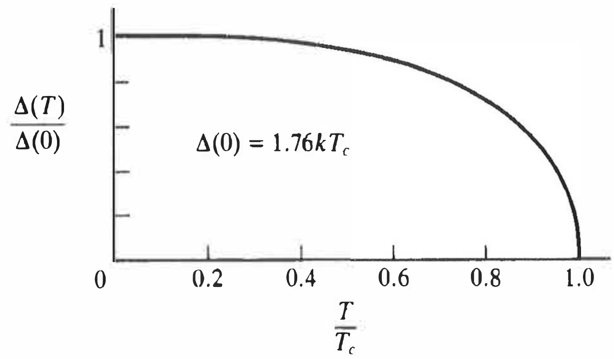

Figure 1.3: Temperature dependence of the energy gap in BCS theory, in the weak-coupling limit (Eq. 1.26). Taken from M. Tinkham, *Introduction to superconductivity*, second ed., McGraw-Hill, Inc. (1996).

which can be diagonalized using the transformations

$$\begin{aligned} c_{\mathbf{k}\uparrow} &= u_{\mathbf{k}}^* \gamma_{\mathbf{k}\uparrow} + v_{\mathbf{k}} \gamma_{\mathbf{k}\downarrow}^+, \\ c_{-\mathbf{k}\downarrow}^* &= -v_{\mathbf{k}}^* \gamma_{\mathbf{k}\uparrow} + u_{\mathbf{k}} \gamma_{\mathbf{k}\downarrow}^+. \end{aligned} \tag{1.24}$$

The diagonalized hamiltonian is

$$H_M = \sum_{\mathbf{k}} (\xi_{\mathbf{k}} - E_{\mathbf{k}} + \Delta_{\mathbf{k}} b_{\mathbf{k}}^*) + \sum_{\mathbf{k}} E_{\mathbf{k}} (\gamma_{\mathbf{k}\uparrow}^+ \gamma_{\mathbf{k}\uparrow} + \gamma_{\mathbf{k}\downarrow}^+ \gamma_{\mathbf{k}\downarrow}), \tag{1.25}$$

with all the quantities identical with the ones defined previously. Now it becomes obvious that the Fermi operators $\gamma_{\mathbf{k}\uparrow,\downarrow}$ describe elementary excitations above the $|BCS\rangle$ ground state, *quasiparticle excitations*, with the energy $E_{\mathbf{k}} = (\xi_{\mathbf{k}}^2 + |\Delta_{\mathbf{k}}|^2)^{1/2}$. Using the previous definition we can write

$$\Delta_{\mathbf{k}} = -\sum_{\mathbf{l}} V_{\mathbf{k},\mathbf{l}} \langle c_{-\mathbf{l}\downarrow} c_{\mathbf{l}\uparrow} \rangle = -\sum_{\mathbf{l}} V_{\mathbf{k},\mathbf{l}} u_{\mathbf{l}}^* v_{\mathbf{l}} \langle 1 - \gamma_{\mathbf{l}\uparrow}^+ \gamma_{\mathbf{l}\uparrow} - \gamma_{\mathbf{l}\downarrow}^+ \gamma_{\mathbf{l}\downarrow} \rangle.$$

Since $\langle \gamma_{\mathbf{l}\uparrow,\downarrow}^+ \gamma_{\mathbf{l}\uparrow,\downarrow} \rangle$ is nothing else but the average population of that specific quasiparticle level, $f(E_{\mathbf{k}}) = (e^{\beta E_{\mathbf{k}}} + 1)$, with $\beta = 1/k_B T$, transforming the summation into an integral in the equation above, we can write an equation for the temperature dependent value of Δ:

$$\frac{1}{N(0)V} = \int_0^{\hbar\omega_c} \frac{\tanh \frac{1}{2}\beta(\xi^2 + \Delta^2)^{1/2}}{(\xi^2 + \Delta^2)^{1/2}} d\xi, \tag{1.26}$$

which is shown in Fig. 1.3.

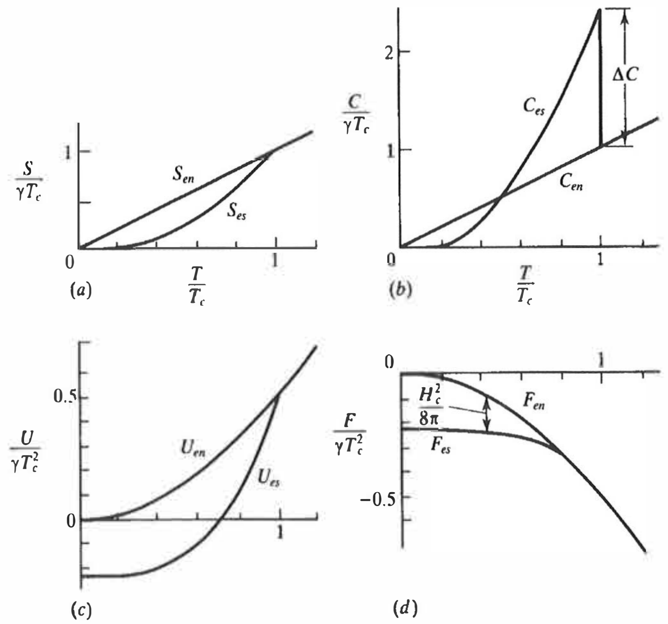

Figure 1.4: Comparison of thermodynamic quantities in superconducting and normal states. S, C, U, F, and H_c are the entropy, the heat capacity, the free energy, and the critical magnetic field, respectively. The subscript *en* refers to the normal electron state quantities, while *es* refers to the superconducting ones, and γ is related to the specific heat of the normal state in the low temperature limit by the formula $C = \gamma T$. $U_{\mathrm{en}}(0)$ is chosen as the zero of ordinate in **(c)** and **(d)**. Because the transition is of second order, the quantities S, U, and F are continuous at the transition temperature, T_{c}. Moreover, the slope of F_{es} joins continuously to that of F_{en} at T_c, since $\partial F/\partial T = -S$. Taken from M. Tinkham, *Introduction to superconductivity*, second ed., McGraw-Hill, Inc. (1996).

At this stage it is possible to calculate thermodynamical quantities. At the transition temperature, the first derivatives of the thermodynamical potential (the free energy), are continuous, while the specific heat, which is a second order derivative, is discontinuous (see Fig. 1.4).

The density of states can be easily calculated using the formula

$$N_{\mathrm{s}}(E)dE = N_{\mathrm{n}}(\xi)d\xi$$

and we obtain the result:

$$\frac{N_{\mathrm{s}}(E)}{N(0)} = \frac{d\xi}{dE} = \begin{cases} \frac{E}{\sqrt{E^2-\Delta^2}} & (E > \Delta) \\ 0 & (E < \Delta) \end{cases} . \tag{1.27}$$

As mentioned before, we observe the formation of an energy gap around the Fermi energy. Due to this gap in the energy spectrum, the electrons can move without being scattered and the resistance of the sample becomes zero.

According to the knowledge of the author, in all the other higher order phase transitions the discontinuous derivatives have infinite jumps. The existence of such infinite discontinuities makes the application of the Ehrenfest's equations and, as a consequence, the Ehrenfest's classification for the phase transitions, impossible. In this case, the theory of Tisza is applicable.[2]

1.3 Mesoscopic systems

A mesoscopic system is defined as one in which some of the dimensions are comparable to the characteristic microscopic lengths, the choice of which depends on the system and on the phase under study. Using as examples the systems analyzed in the papers of this thesis, the characteristic microscopic length can be the dominant phonon wave-length, if one studies the thermal properties of a dielectric, the Fermi wave-length, if a system of fermions is investigated, or the coherence length, if one describes a superconductor. The property of extensivity, characterizing the bulk systems, can be lost in mesoscopic systems and the parameters that are defined as intensive in the bulk, could depend on the dimensions. Due to this, the phases do not have precise definitions any more, and the boundaries between them become vague. For example, if we focus on the Bose condensation of a fixed finite number of particles in boxes with small dimensions, or in harmonic traps, we observe a change in the specific heat of the system, as a function of temperature. This change is most pronounced in a range of temperatures close to the condensation point.

We will first analyze the case in which a Bose gas is confined inside a cuboidal box, with dimensions $l_1 \gg l_2 \gg l_3$. This case was studied by Sonin in [12], and he was the first to point out that in such deformed systems the Bose-Einstein condensation can take place in steps, from the three dimensional distribution to the ground state, obtaining in between two-dimensional and/or one-dimensional macroscopic populations. This concept was much later called *Multiple-step Bose-Einstein condensation* (MSBEC), when it was rediscovered, for the case of harmonic traps, by van Druten and Ketterle [13]. If we impose periodic boundary conditions on the walls of the container, in the limit where $l_1, l_2, l_3 \gg \lambda$ (λ is the thermal wave-length, as defined previously), we can write the total number of particles as an obvious sum:

$$
\begin{aligned}
N &= N_0 + N_1 + N_2 + N_3, && (1.28)\\
N_0 &= \frac{z}{1-z}, && (1.29)\\
N_1 &= \sum_{\substack{i=-\infty \\ (i\neq 0)}}^{\infty} z\left[\exp\left(\pi\frac{\lambda^2}{l_1^2}i^2\right) - z\right]^{-1} \approx \frac{l_1}{\lambda}\coth\left[\sqrt{\pi(1-z)}\frac{l_1}{\lambda}\right]\sqrt{\frac{\pi}{1-z}}
\end{aligned}
$$

[2]We do not go here into details, but the interested reader can find a nice introduction into this theory in the book byCallen [2].

$$
-\frac{z}{1-z} = \begin{cases} \frac{\pi}{3}\frac{l_1^2}{\lambda^2}, & (1-z)^{1/2} \ll \frac{\lambda}{l_1} \\ \frac{l_1}{\lambda}\sqrt{\frac{\pi}{1-z}}, & (1-z)^{1/2} \gg \frac{\lambda}{l_1} \end{cases}, \tag{1.30}
$$

$$
\begin{aligned}
N_2 &= \sum_{\substack{k=-\infty \\ (k\neq 0)}}^{\infty} \sum_{i=-\infty}^{\infty} z\left[\exp\left(\pi\frac{\lambda^2}{l_1^2}i^2 + \pi\frac{\lambda^2}{l_2^2}k^2\right) - z\right]^{-1} \\
&\approx -2\frac{l_1 l_2}{\lambda^2} \times \ln\left(\frac{\lambda}{l_2}\sqrt{z} + \sqrt{\frac{\lambda^2}{l_2^2}z + 1 - z}\right) \qquad (1.31) \\
&= \begin{cases} 2\frac{l_1 l_2}{\lambda^2}\ln\frac{l_2}{\lambda}, & (1-z)^{1/2} \ll \frac{\lambda}{l_1} \\ \frac{l_1 l_2}{\lambda^2}\ln\frac{1}{1-z}, & (1-z)^{1/2} \gg \frac{\lambda}{l_1} \end{cases}, \\
N_3 &= \sum_{\substack{n=-\infty \\ (n\neq 0)}}^{\infty} \sum_{k=-\infty}^{\infty} \sum_{i=-\infty}^{\infty} z\left[\exp\left(\pi\frac{\lambda^2}{l_1^2}i^2 + \pi\frac{\lambda^2}{l_2^2}k^2 + \pi\frac{\lambda^2}{l_3^2}n^2\right) - z\right]^{-1} \\
&\approx \frac{2}{\sqrt{\pi}}\frac{l_1 l_2 l_3}{\lambda^3}\int_0^\infty \frac{z\sqrt{t}\,dt}{e^t - z} = \frac{l_1 l_2 l_3}{\lambda^3}\Gamma\left(\frac{3}{2}\right) g_{3/2}^{(-)}(\alpha), \qquad (1.32)
\end{aligned}
$$

where $z = e^{\beta\mu}$ is the fugacity, $\alpha = -\beta\mu$, and $g_m^{(-)}(\alpha)$ is the polylogarithmic function of order m and of argument e^α [14]. The superscript $(-)$ is used to denote the difference between these functions and those that will appear in the case of fermions, where the superscript $(+)$ will be used. The expressions above are deduced in the approximation $z \approx 1$. If we call N_0, N_1, N_2, and N_3 the population of *zero-, one-, two-*, and *three-dimensional phases*, respectively, and the aggregates $N_{(1)} = N_1 + N_0$, $N_{(2)} = N_2 + N_{(1)}$, and $N_{(3)} = N_3 + N_{(2)} = N$ the population of *one-, two-*, and *three-dimensional gases*, respectively, then we can deduce the temperature of the i-dimensional Bose condensation from the condition that the population of the i-dimensional phase is equal to the number of particles of the i-dimensional gas in the limit $z \dashrightarrow 1$ (corresponding to the first branches in the final approximations used in Eqs. (1.30) and (1.31)).

Since the 3D condensation is well known, let us analyze shortly a 1D and a 2D gas with particle numbers $N_{(1)}$ and $N_{(2)}$, respectively. In the 1D case, at the condensation temperature $T_{c,1}$, which corresponds to the thermal wave-length $\lambda_{c,1}$, we have the equation

$$
\begin{aligned}
N_{(1)} &\equiv \frac{\pi}{3}\frac{l_1^2}{\lambda_{c,1}^2} \qquad (1.33) \\
&= \frac{l_1}{\lambda_{c,1}}\coth\left[\sqrt{\pi(1-z)}\frac{l_1}{\lambda_{c,1}}\right]\sqrt{\frac{\pi}{1-z}}.
\end{aligned}
$$

Using the notation $\xi_1 \equiv \sqrt{1-z}(l_1/\lambda_{c,1})$ we obtain an equation which is independent of the dimension of the sample and of the temperature:

$$\frac{\sqrt{\pi}}{3} = \frac{\coth\left(\sqrt{\pi}\xi_1\right)}{\xi_1}, \tag{1.34}$$

and which has the solution $\xi_1 \approx 1.7$. Therefore, the condition imposed in the definition of the condensation temperature, $(1-z)^{1/2} \ll \frac{\lambda}{l_1}$, is not satisfied. Moreover, we observe that at the temperature $T_{c,\ 1}$,N_0 is of the same order as $N_{(1)}$. Therefore this can not be a proper, sharp phase transition.

In order to study the 2D situation, we define $\xi_2 \equiv \sqrt{1-z}(l_2/\lambda)$. The condensation temperature $T_{c,2}$ can be calculated in a similar way, by writing

$$\begin{aligned} N_{(2)} &\equiv 2\frac{l_1 l_2}{\lambda_{c,2}^2} \log \frac{l_2}{\lambda_{c,2}} \\ &= 2\frac{l_1 l_2}{\lambda_{c,2}^2} \log \frac{\frac{l_2}{\lambda_{c,2}}}{\sqrt{z}\left(1+\sqrt{1+\frac{1-z}{z}\frac{l_2^2}{\lambda_{c,2}^2}}\right)} + \frac{l_1}{\lambda_{c,2}}\sqrt{\frac{\pi}{1-z}}. \end{aligned} \tag{1.35}$$

In the limit $l_1/\lambda_{c,2} \gg 1$ the equation above can be reduced to a universal form:

$$2\xi_2 \log \frac{1+\sqrt{1+\xi_2^2}}{2} = \sqrt{\pi}, \tag{1.36}$$

with the solution $\xi_2 \approx 1.9$. Again, the condition imposed in thc first branch of the last form of Eq. (1.31), namely $(1-z)^{1/2} \ll \frac{\lambda}{l_1}$, is not satisfied. At the condensation temperature,

$$N_1(T_{c,2}) = \frac{\sqrt{\pi}}{\xi_2}\frac{l_1 l_2}{\lambda_{c,2}^2},$$

which means that a finite 2D population is condensed onto the 1D phase. Nevertheless, since the 2D density of particles has to diverge as $\log(l_2/\lambda)$ when l_2 increases to infinity (bulk limit), in order to have a finite condensation temperature in this limit, the ratio N_1/N_2, at $T_{c,2}$ converges to zero. This means that the function $N_2(T)$ is not analytical at $T = T_{c,2}$.

We reach the conclusion that N_3 and N_2 are not analytical functions of T at the condensation temperatures $T_{c,3}$ and $T_{c,2}$, respectively, while N_1 and N_0 are analytical below $T_{c,2}$ (see Fig. 1.5). In any case $T_{c,\ 1}$and $T_{c,2}$ do not represent proper phase transformations, since in the 1D or 2D bulk limits, respectively, the particle densities should diverge in order to have a non-zero condensation temperature. In usual 3D bulk systems, where $l_{1,2,3} \to \infty$, such that, in the limit, $l_i/l_j > 0$, for any $i, j \in \{1, 2, 3\}$, the 3D condensation happens first, triggering the 2D and 1D condensations at the same time. In the case of small, finite systems, which are very deformed (for example, there exist l_i and l_j, such that $l_i/l_j \to \infty$), the 3D condensation might not trigger the condensation of (some of) the lower dimensional gases. In such a case, the gas condenses into a lower dimensional one, and not into the ground state. In this case we have a multiple-step Bose-Einstein condensation (BEC), according to the terminology introduced in [13]. In Fig. 1.5, from Ref. [12] one can see the dependence on temperature of the numbers of particles in the one-, two-, and three-dimensional phases and gases. The first order derivatives of N_2 and N_3 have finite jumps at $T_{c,2}$ and $T_{c,3}$, respectively, as discussed before.

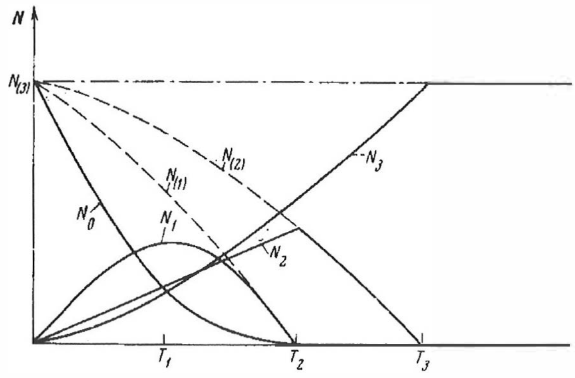

Figure 1.5: The dependence on the temperature of the numbers of particles in the 1, 2, and 3D phases (continuous lines) and gases (dashed lines). Taken from E. B. Sonin, Sov. Phys. JETP **29**, 520 (1969).

The realization of BEC in ultracold atoms in magnetic traps has opened up far-reaching new prospects. This led to the rediscovery of MSBEC in harmonic traps by van Druten and Ketterle [13]. Generalizing the definition given in the previous section, in such a trap, the d-dimensional thermodynamic limit is taken such that $N \to \infty$, while the characteristic frequencies of the trap decrease to zero, in such a way that $N \prod_{i=1}^{d} \omega_i$ remains finite. It is easy to show that, in this limit, BEC exists for $d \geq 2$ (the situation for $d = 3$ was discussed in Section 1.2). For $d = 1$ a BEC temperature, $T_{c,1,h}$ can be defined in finite systems by the relation [15]:

$$N = \frac{k_B T_{c,1,h}}{\hbar\omega_1} \log\left(\frac{2k_B T_{c,1,h}}{\hbar\omega_1}\right), \tag{1.37}$$

in a similar way as in the case of cuboidal boxes. If the trap is very asymmetric, so that $T_{c,1,h} < T_{c,3,h}$ for the number of particles in the trap ($T_{c,3,h}$ is the 3D condensation temperature), the MSBEC can be observed, first from 3D to 1D, and then from 1D to 0D, as shown in Fig. 1.6 [13].

In the cases investigated the lower dimensional gases always condense at lower temperatures than the higher dimensional ones, with which they coexist. On the

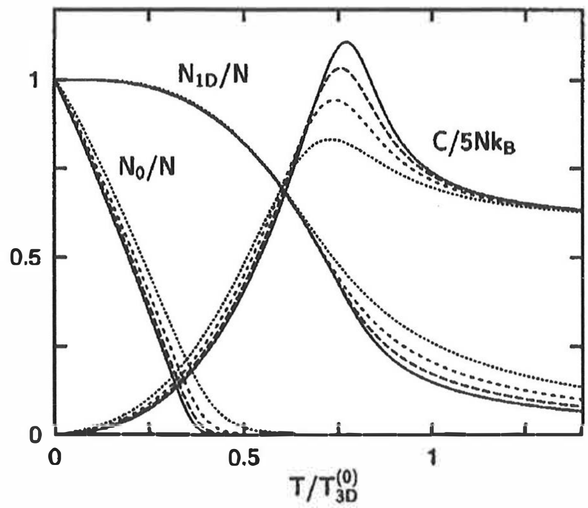

Figure 1.6: Behaviour of the ideal Bose gas in a harmonic trap with $\omega_1 \ll \omega_2 = \omega_3$ for different particle numbers, $N = 10^4$ (dotted), 10^6 (short dashed), 10^8 (long dashed), and 10^{10} (solid lines). The condensation temperatures were kept fixed $3T_{\mathrm{c,1,h}} = T_{\mathrm{c,3,h}}$. Shown are the ground state fraction, N_0/N, the fraction of population excited in the ω_1 direction, $N_{1\mathrm{D}}/N$, and the specific heat per particle, $C/5Nk_{\mathrm{B}}$. Taken from N. J. van Druten and W. Ketterle, Phys. Rev. Lett. **79**, 549 (1997).

other hand, if one of the dimensions of a system is very much reduced (or one of the three frequencies that characterize a harmonic trap is increased very much), the degree of freedom corresponding to this dimension can freeze out before BEC or MSBEC happens. In this case we have a Bose-like condensation (BLC). This phenomenon will be presented in section 2.1 and it turns out that it is common to both bosons and fermions (see Paper III), and, moreover, appears also in systems of massless particles, like phonons (Paper I and Paper II).

The first important steps in the study of the effect of the finiteness of the dimensions of the box on the shape of the peak accompanying the Bose condensation were made by Goble and Trainor. In [16, 17] they calculated numerically the specific heat of systems of bosons in cuboidal boxes of dimensions $l_1 \times l_2 \times l_3$, with $l_{1,2} \gg l_3$, for various boundary conditions. The general observation was that, as the dimension l_3 decreases, the cusp-like maximum of the specific heat corresponding to the BEC temperature (see Fig. 1.2) is rounded off and the maximum of the specific heat moves towards higher temperatures. Nevertheless, the position and the height of this maximum depends upon the boundary conditions imposed on the walls. But, as mentioned in [17], the most striking observation was that, for Dirichlet boundary conditions, the height of the maximum first increases with the decrease of l_3 and then decreases again. Although not clearly identified, the MSBEC was already emphasized in these works, which appeared earlier than Sonin's [12].

Using a technique developed by Krueger [18], Pathria and Greenspoon [19, 20, 21, 22] calculated analytically, in different perturbation orders, the specific heat of a system of bosons in cuboidal boxes of finite dimensions and with different boundary conditions on the walls. The conclusion was that the increase of the height of the maximum in the specific heat at the condensation temperature is an effect of the boundary conditions employed, and it happens just in the case of Dirichlet boundary conditions. In all the other cases that were calculated, the height of the maximum was decreasing with the decrease of the dimensions of the system (see Fig. 1.7). In contradiction with this conclusion, I shall show later that, if one employs periodic boundary conditions on the walls of a container with the dimensions $l_1 \gg l_2 = l_3$, the height of the maximum of the specific heat is decreasing in the beginning, with decreasing l_2 and l_3, and then increases monotonically, as $l_2, l_3 \to 0$, towards a maximum which is higher than the bulk value and, moreover, higher than the value obtained in the case of Dirichlet boundary conditions (Fig. 2.5) (Paper III). In any case, Pathria and Greenspoon could not observe this, since their approximation technique would fail when the dimensions of the system decrease too much and when the system enters the region of observability of Bose-like condensation (Paper I, Paper II, and Paper III).

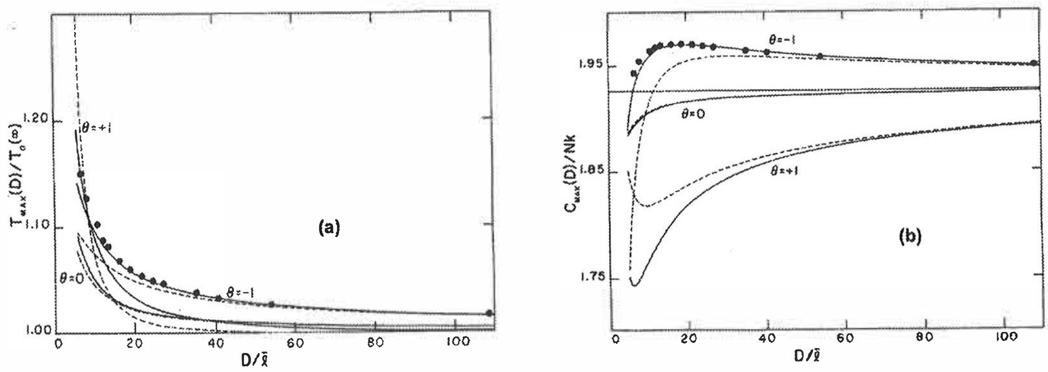

Figure 1.7: Temperature $T_{\max}(D)$ at which the specific heat of an infinite slab of thickness D is maximum **(a)**, and the height $C_{\max}(D)$ of this maximum **(b)**: first order results, dashed lines; second-order results, solid lines. The variable θ is used to specify the boundary conditions: -1 for Dirichlet, 0 for periodic and 1 for Neumann boundary conditions. The results of Goble and Trainor [17] are shown as filled circles. Taken from S. Greenspoon and R. K. Pathria, Phys. Rev. A **8**, 2657 (1973).

In the case of traps, the finiteness of the trap frequencies and of the number of particles introduce a shift towards lower values in the 3D condensation temperature, as compared to condensation temperature in the thermodynamic limit [10] (that is, in the opposite direction from the case of boxes):

$$T_{\mathrm{c,3,h}} \approx \frac{\hbar}{k_{\mathrm{B}}} \left(\frac{\omega_1 \omega_2 \omega_3 N}{\zeta(3)}\right)^{1/3} \left(1 - \frac{\gamma\zeta(2)}{3\zeta(3)^{2/3}} \frac{1}{N^{1/3}}\right). \tag{1.38}$$

The parameter γ is equal to $2/3$ in the case of an isotropic trap, and has to be computed numerically for the anisotropic cases. As the particle number decreases, the maximum of the specific heat at the condensation temperature decreases and the curve becomes smoother. These effects can be observed in Fig. 1.6.

1.4 Clusters

Clusters can be defined as a small, bounded group of atoms. The number of atoms usually ranges from a few (a small molecule) up to a few thousands. The forms that clusters exhibit may have characteristics that justify us to call them *phases* or *phase-like forms*. The simplest and most common examples of such phases are those of cold solid and warm liquid clusters. The particles that form a solid cluster vibrate with small amplitudes (compared with the nearest neighbour distance) around their equilibrium sites. On the other hand, in a warm liquid, the particles exhibit diffusive motion that can be quantified by evaluating their mean-square displacement vs. time; the slopes of such curves are nearly constant over distances and times that are large compared with the amplitudes and periods of vibrations around equilibrium sites, but smaller than the dimensions of the cluster and the time required for the diffusive transit of the cluster [5].

In a bulk system, the exchange of particles between two or more coexisting phases is negligible as compared with the total particle number and therefore does not affect its thermodynamic properties. From the macroscopical point of view, the system is in equilibrium. In clusters, the fraction of particles that pass from one phase to another cannot be neglected. Therefore an equilibrium cannot be achieved, and the denomination of *phase-like form* is more adequate. The concentrations of different phase-like forms in the cluster vary with time and the dynamic equilibrium attained can be described in terms of averages over *long* time or by statistical ensembles. The two averages should give the same results, in the assumption that the system is ergodic.

The diffusivity of the particle motion mentioned above is not all the time a good tool to diagnose the phase-like form of a cluster. In order to do this, one can employ other methods, like the study of the *velocity autocorrelation functions* and their Fourier transforms, the *pair correlation functions*, the *angular correlation functions*, the *root-mean-square fluctuation of the nearest-neighbour distance*, δ, etc. If one uses the pair and angular correlation functions, a solid cluster exhibits very sharp peaks, as a crystalline or quasicrystalline solid do, while a liquid cluster shows much broader peaks in distribution, beyond the first-neighbour shell. The ratio δ between the root-mean-square fluctuations and the nearest-neighbour distance is below about 0.1 in the case of a solid, and typically above 0.2 for liquids (*Lidemann criterion*).

In Ref. [5], Berry gave a list of known or potential phase-like forms, that we reproduce in Table 1.1 (by LJ_6 we denote a Lennard-Jones cluster composed of six atoms). The solid and liquid phase-like forms were already described. In the

Table 1.1: The *menagerie of phase-like forms* that clusters may exhibit.

Form	Special Condition	Example
Solid	lowest temperature	all, except He and possibly H_2
Liquid	none	all except possibly clusters of C_{60}
Surface-melted	liquid wets solid	pairwise Lennard-Jones, Morse
Core-melted (?)	*liquid denser than solid*	*Ga?* H_2O*?*
Soft solid	multiple solid-like minima	LJ_6, Cu_6
Flexible Planar	perhaps repulsive as well as attractive long-range forces	$(KCl)_4, (KCl)_5$
Nonwetted	liquid does not wet solid	$(KCl)_{32}$
Slush	short duration in each phase-like form	Ar_{14}, Ar_{17}

case of a *surface-melted cluster*, the outermost layer satisfies the conditions for a liquid-like behavior, but the inner layers remain solid. Sometimes, the liquid characteristics of the outer layer are given by a few atoms, so called *floaters*, that pop out of it and move just above the cluster surface.

When the cluster can pass from its lowest energy configuration into a limited number of others, going through relatively large amplitude motions, but not of any kind that permute identical atoms among nonequivalent sites, we say that it is in a *soft-solid* phase-like form.

The *planar structures* are exhibited by small alkali halide clusters, that show planar ring and rectangular, or “ladder”, structures at energies somewhat above the energies of their rock-salt like global minima.

When the liquid forms do not wet their parent solids, as in the case of alkali halides, part of the cluster may be a regular solid and the other part an amorphous liquid, but the liquid constitutes one side of the cluster and not its surface. In this case we have a *nonwetted form.*

We say that we discuss a *slush* when the passage between phase-like forms is too frequent and the properties of any phase-like forms cannot be established.

As the last example we discuss the *core-melted* cluster, since it was not previously observed before in simulations or in experiments. It should consist of a liquid core and a solid outer shell. In Chapter 4 we show that such a phase-like form exists and it can be obtained using a special kind of interaction potential [23]. Moreover, it turns out that the Menagerie should be completed with the *core-surface melted* phase-like form, in which the core and the surface are liquid, while the particles in between form a solid. Also, due to the nature of this new interaction, besides what we could call "the usual" liquid-like form, a *dense liquid-like* form can exist at lower temperatures [23].

Chapter 2

New transitions and special effects characteristic to restricted geometries

2.1 Bose-like condensation

2.1.1 Massless bosons: phonon gases

In Section 1.2, the phenomenon of Bose-Einstein condensation (BEC) was discussed. This condensation was identified with a phase transition of order one, during which a finite part of the bosonic gas condenses into the ground state. When some of the dimensions of the system are decreased, the Bose gas may condense in steps towards the ground state, exhibiting in between macroscopic one- and/or two-dimensional populations. If the finite dimensions of the system are reduced further (or the particle density is reduced), the BEC condensation temperature may be exceeded by the temperature at which some of the degrees of freedom of the gas are frozen out. Although this phenomenon was expected to happen (see for example [13]), according to the knowledge of the author, nobody investigated it theoretically or experimentally before us [Paper I].

In experiments done on ultrathin dielectric membranes (thickness: $l_3 \approx 200$ nm) made of silicon nitride, it turned out that the heat conductivity κ is roughly proportional to T^2 [24]. Moreover, when the membrane was cut and the heat conductivity of narrow bridges was measured, it was observed that the heat conductivity depends on the width of the bridge, l_2, much more strongly than expected (for example, if the mean free path of the phonons in the membrane would be much smaller than the width of the bridge, κ should be constant), and the exponent of the temperature dependence of κ decreases also when the width decreases (see Fig. 2.1 from [25]).

In the usual picture, when the phonon gas distribution in the membrane is three-dimensional, the heat conductivity is related to the heat capacity and the

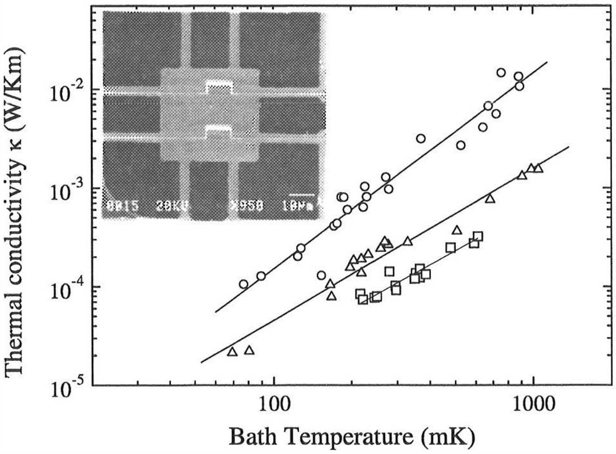

Figure 2.1: Effective thermal conductivity as a function of temperature for silicon nitride membranes of about 250 nm thickness in three different geometries: full membrane (circles), membrane with 25 μm wide bridges (triangles), and membrane with 4 μm wide bridges (squares). Inset: measurement geometry with the 4 μm bridges. The heater and the thermometer are located on the membrane. Taken from J. P. Pekola, A. J. Manninen, M.M. Leivo, K. Arutyunov, J.K. Suoknuuti, T.I. Suppula, and B. Collaudin, accepted for publication in Physica B.

mean free path by the relation [26]:

$$\kappa = \frac{1}{3} cvl, \tag{2.1}$$

where c is the heat capacity, v is the average sound velocity, and l is the mean free path of the phonons. A heat conductivity proportional to T^2 would correspond to a mean free path proportional to the wave-length of the phonons, λ. On the other hand, the strong decrease of the heat conductivity with the bridge width suggests that the mean free path in the membrane (hence without considering the scattering on the surfaces), Λ, is longer than l_2, while from the decrease of the exponent one can conclude that the scattering on the bridge edges is not perfectly diffuse, but the phonons may undergo many reflections until they are scattered. According to the experimental data, this mechanism would produce a new mean free path, proportional to λ^p, with $p > 1.5$. Considering the dimensions of the membrane (400×400 $\mu\mathrm{m}^2$) and of the bridges (for example $l_1 \times l_2 = 100 \times 25$ $\mu\mathrm{m}^2$), and the fact that the measurements were done over a large temperature range (wider than one order of magnitude) – see Fig. 2.1 – we can conclude that the mean free path in the membrane material, at the dominant frequency, is bigger than half the width of the membrane, at least in the lower part of the temperature interval. This brings us to the ballistic limit of heat transport and to the next point of our discussion.

When Λ is longer than the membrane dimensions or the mean free path that results from the scattering on the membrane surfaces, L, one can employ a model analogous to the radiative transfer between two black bodies (see [27] and the references therein). In this model, the heat flow through the unit area is written in the form

$$\phi = 4\sigma T^3 \xi, \tag{2.2}$$

where σ is the Stefan-Boltzmann constant for the phonon gas and ξ is a numerical factor smaller or equal to one, which gives the reduction of the heat flow due to the diffuse scattering on the surface. For a perfectly specular surface $\xi = 1$, while for a perfectly diffusive surface ξ assumes its lowest value. From Eq. (2.2) one can see that in the ballistic limit that we discussed in the previous paragraph $\xi = 1$ and $\kappa \propto T^3$. This is in contradiction with the experimental observation.

To solve this problem one should observe that the dominant frequency of the 3D distribution of phonons in silicon-nitride, $\bar{\omega}$, calculated by the formula $\hbar\bar{\omega} \approx 1.6 k_{\mathrm{B}} T$ [26], is approximately $\bar{\omega} \approx 2.1 \times 10^{11} \times T$ ($\mathrm{s}^{-1}\mathrm{K}^{-1}$). On the other hand, assuming Neumann boundary conditions on the membrane surfaces and using the average velocity of sound in silicon-nitride, which is $v_{\mathrm{s}} \approx 7200$ m/s, one can calculate the minimum frequency of phonons in the z direction, perpendicular to the membrane surface: $\omega_{3_{min}} = v_s \times (\pi/l_3) \approx 1.1 \times 10^{11}$ s^{-1} (where $l_3 = 200$ nm). We then conclude that for $T \leq 0.5$ K, $\bar{\omega} < \omega_{3_{min}}$ and the approximation of a "continuous" spectrum in the z direction is not justified. Therefore all the thermodynamic quantities should be calculated maintaining the discrete summation of the phonon modes perpendicular to the membrane surfaces (see Paper I). If we take into account the mean free path of the phonons in the membrane and the probability of diffuse scattering on the membrane surface, we obtain the following expressions for the heat capacity and heat conductivity of the membrane:

$$C = \frac{3k_B S}{2\pi}\left(\frac{k_B T}{v_s \hbar}\right)^2 \left[\int_0^\infty \frac{x^3 e^x}{(e^x-1)^2}\mathrm{d}x + \sum_{n=1}^{\infty}\int_{nx_0}^{\infty}\frac{x^3 e^x}{(e^x-1)^2}\mathrm{d}x\right], \tag{2.3}$$

$$\begin{aligned}\kappa &= \frac{3}{4\pi}\frac{k_B^3 T^2}{\hbar^2 v_s}\left(\frac{k_B T}{\hbar v_s}\right)^{-l} C_l \times \\ &\sum_{n=0}^{\infty}\int_{nx_0}^{\infty}\mathrm{d}x \frac{x^{1-l}(x^2 - n^2 x_0^2)}{1 + C_s C_l n \left(\frac{k_B T}{\hbar v_s}\right)^{2-l}\frac{x_0 x^{1-l}}{l_3}}\frac{e^x}{(e^x-1)^2},\end{aligned} \tag{2.4}$$

where x_0 is a dimensionless parameter:

$$x_0 = \frac{\pi\hbar}{k_B T}\frac{v_s}{l_3}, \tag{2.5}$$

and the other parameters, together with the approximations used, are explained in Paper I. If we write $C \propto T^{p_C}$ and $\kappa \propto T^{p_\kappa}$, the exponents of the temperature dependence can be calculated by the formulae

$$p_C = T\frac{\partial}{\partial T}(\ln C) \tag{2.6}$$

and

$$p_\kappa = T\frac{\partial}{\partial T}(\ln \kappa). \tag{2.7}$$

In this way we obtain

$$p_C = 2 + \frac{\sum_{n=1}^{\infty} \frac{(nx_0)^4 \exp(nx_0)}{[\exp(nx_0)-1]^2}}{\int_0^\infty \frac{x^3 e^x}{(e^x-1)^2}\mathrm{d}x + \sum_{n=1}^{\infty}\int_{nx_0}^{\infty}\frac{x^3e^x}{(e^x-1)^2}\mathrm{d}x} \tag{2.8}$$

and

$$\begin{aligned} p_\kappa = {} & (2-l) + \\ & \left\{\sum_{n=1}^{\infty}\int_{nx_0}^{\infty}\mathrm{d}x\frac{2(nx_0)^2x^{1-l} + C_sC_l\left(\frac{k_BT}{\hbar v_s}\right)^{2-l}\frac{(nx_0)x^{2-2l}}{l_3}((nx_0)^2+x^2)}{\left[1+C_sC_l\left(\frac{k_BT}{\hbar v_s}\right)^{2-l}\frac{(nx_0)x^{1-l}}{l_3}\right]^2}\right. \\ & \left.\times\frac{e^x}{(e^x-1)^2}\right\} \\ & \times\left\{\sum_{n=0}^{\infty}\int_{nx_0}^{\infty}\mathrm{d}x\,\frac{x^{1-l}(x^2-(nx_0)^2)}{1+C_sC_l\left(\frac{k_BT}{\hbar v_s}\right)^{2-l}\frac{(nx_0)x^{1-l}}{l_3}}\,\frac{e^x}{(e^x-1)^2}\right\}^{-1}. \end{aligned} \tag{2.9}$$

The results, in the case of perfectly specular boundary conditions, are plotted in Fig. 2.2. We can observe here the crossover between the 2D and 3D phonon gas distributions, the first one corresponding to the low temperature range and the second one being observed at higher temperature. The dimensionality is reflected in the value of these exponents.

Using the integer l and the constant C_l that enter in the expression of the mean free path, as fitting parameters, we obtained good agreement with the experimental observations (see Fig. 2.3) for $l = 0$ and $C_0 = \Lambda \approx 10.3\ \mu$m (see Paper I for more details about the fitting procedure). It appears that the mean free path of the phonons in the membrane is almost independent of the wavelength, at low temperatures. Nevertheless, one can see a slight tendency to a negative curvature in κ vs. T in the central part of Fig. 2.3, which could be explained by a cross-over of different scattering mechanisms with different l. As a check we made the fit for $l = 1$, for which we obtained $C_l \approx 101.9$. The curves marked by (2) in Fig. 2.3 correspond to κ and p_κ calculated for these values of l and C_l. We should expect that mechanisms involving larger l start to contribute

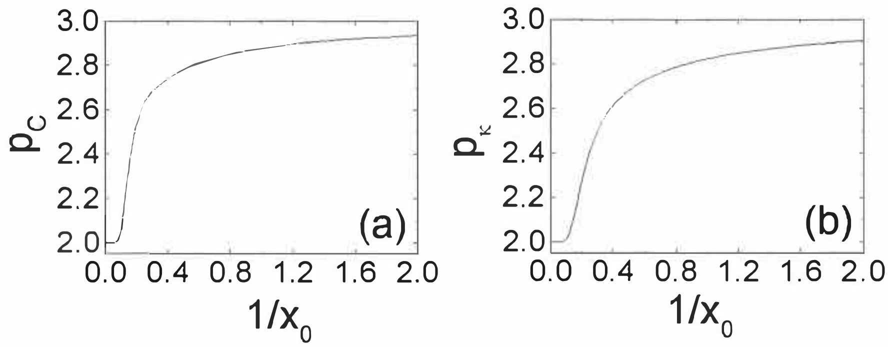

Figure 2.2: The exponent of the temperature dependence as a function of $1/x_0$ ($1/x_0 \propto T$) for: a) the specific heat; b) the heat conductance, in the case of perfectly specular surfaces.

to Λ as the temperature is increased. This should cause a downward bending of the experimental curve representing κ. This tendency was observed also in other samples measured, and it seems to show up in the crossover region, but no systematic investigation was made in this respect.

In the inset of Fig. 2.3 we plot the exponents of the temperature dependence of κ for the two values obtained for l. As the diffusivity of the surface increases, the transition from 2D to 3D phonon gas becomes smoother. The exponent can even decrease with the increase of temperature in some interval above the crossover region (but cannot become smaller than 2). Keeping in mind the correspondence between the value of the exponent and the dimensionality d of the phonon gas distribution, we can say that the conductivity in the membrane may behave as in the 2D case (as it happens in our situation for $l = 0$) even above the crossover region, as this is defined using the exponent p_C.

An extension of this analysis to the case of bridges and small particles was made in Paper II. The change in the dimensionality of the phonon gas distribution from three to one and even down to zero has been discussed there. We called this change in dimensionality *Bose-like condensation* (BLC), because of a direct analogy with the multiple-step Bose-Einstein condensation (MSBEC), introduced in Section 1.3. During the BLC, the population of the energy levels which are excited in the direction of the restricted dimensions (say, perpendicular to the membrane surface), or the 3D phase, in the terminology introduced in the section mentioned before [12], decreases and a lower dimensional distribution becomes

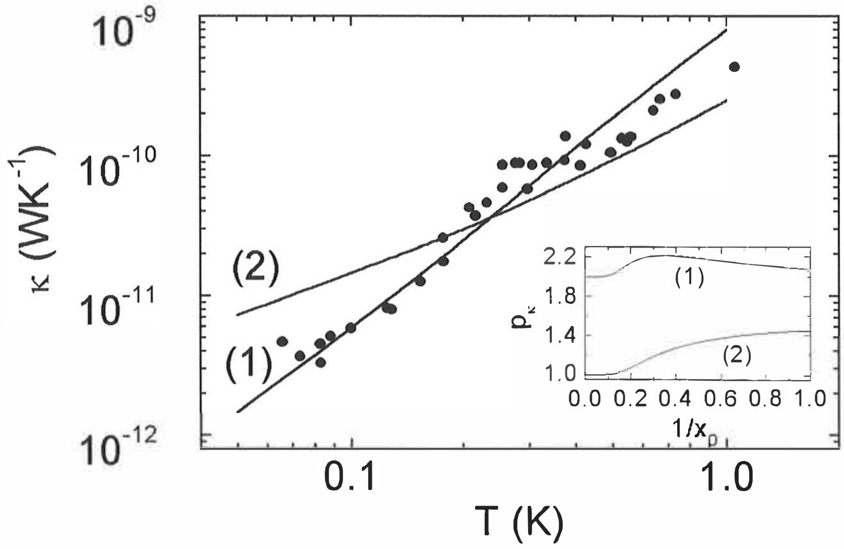

Figure 2.3: The experimental data (the dots) and the theoretical calculations [solid lines – Eq. (2.4)] for curve (1): $l = 0$ and $C_l \approx 10.3 \times 10^{-6}$ (m); curve (2): $l = 1$ and $C_l \approx 101.9$. We used $v_s = 7200$ ms^{-1}, $l_3 = 200$ nm and $C_s \approx 5 \times 10^{-17}$ m^2. The inset shows the exponents of the temperature dependence of κ [Eq. (2.9)] corresponding to the curves (1) and (2) in the main figure.

"macroscopical". This phenomenon produces qualitatively new features in the quantities that can be measured experimentally.

In all the models presented above, the material from which the membrane and the bridges were made was considered homogeneous. All the fluctuations that might occur in the density or in the coupling strength between the atoms were ignored, as well as the fact that the silicon-nitride is a composite material. All these facts may complicate the dispersion relation of the phonons. Also, the finite geometries would modify the phonon modes from the simple plane-wave form that we used in Paper I and Paper II.

2.1.2 Massive particles

Bose-like condensation occurs also in the case of massive particles. Moreover, in this case it is similar for both bosons and fermions. The author analyzed this in Paper III in the general case when the particles are described by a mean field hamiltonian of the form $H = H_c + H_d$, with H_c having a (quasi)continuous spectrum $\epsilon_c \in [0, \infty)$ and H_d having discrete eigenvalues ϵ_i, $i = 0, 1, \ldots$. The mean occupation numbers of the single particle energy levels ϵ are $\langle n_\epsilon^{(\pm)} \rangle = (\exp{(\alpha + \epsilon/k_B T)} \pm 1)^{-1}$, where $(-)$ is the superscript for bosons, and $(+)$ for fermions, α has been defined earlier, and μ is the chemical potential. We introduce the functions

$$Z_n^{(\pm)} = \sum_\epsilon \left(\frac{\epsilon}{k_{\rm B}T}\right)^n \langle n_\epsilon^{(\pm)}\rangle, \tag{2.10}$$

$$G_n^{(\pm)} = \sum_\epsilon \left(\frac{\epsilon}{k_{\rm B}T}\right)^n [\langle n_\epsilon^{(\pm)}\rangle \mp \langle n_\epsilon^{(\pm)}\rangle^2] = -\frac{\partial Z_n^{(\pm)}}{\alpha}, \tag{2.11}$$

in a similar way as Pathria and Greenspoon did for bosons in [19]. Then, for example, the number of particles, the internal energy, and the heat capacity can be written as $N^{(\pm)} = Z_0^{(\pm)}$, $U^{(\pm)} = k_{\rm B}TZ_1^{(\pm)}$, and $C_{\rm V}^{(\pm)} = k_{\rm B}(G_2^{(\pm)} - G_1^{(\pm)^2}/G_0^{(\pm)})$, respectively (we shall consider here only spinless particles). To avoid divergent terms that occur in the functions introduced when T approaches zero, in the case when the ground state energy ϵ_0 is positive, we redefine α as $\alpha - \epsilon_0/kT$ and ϵ as $\epsilon - \epsilon_0$. Making these replacements we do not change the thermodynamics of the canonical ensemble. If the density of the energy levels of the (quasi)continuous spectrum, as a function of energy, is $\sigma(\epsilon_{\rm c})$, then we can write

$$Z_0^{(\pm)} = \sum_{i=0}^{\infty} \int_0^\infty \frac{\sigma(\epsilon)}{\exp{(\alpha + \beta\epsilon_i + \beta\epsilon)} \pm 1}\, d\epsilon\,, \tag{2.12}$$

where $\beta = 1/k_{\rm B}T$. If $\alpha \gg 1$ in the temperature range of interest for the study of BLC ($\epsilon_1/k_{\rm B}T \approx 1$), we can write Z_0 in terms of two functions, corresponding to the continuous and to the discrete spectrum, respectively:

$$Z_0^{(\pm)} = e^{-\alpha} Z_{\rm c}^{(\pm)} Z_{\rm d}^{(\pm)}\,, \tag{2.13}$$

where $Z_{\rm c}^{(\pm)} = \int_0^\infty \sigma(\epsilon)e^{-\beta\epsilon}\, d\epsilon$ and $Z_{\rm d}^{(\pm)} = \sum_{i=0}^\infty e^{-\beta\epsilon_i}$. In this approximation there is no difference between bosons and fermions, and according to Eq. (2.11), $G_n^{(\pm)} = Z_n^{(\pm)}$. Using the relation

$$\left(\frac{\partial^n Z_n^{(\pm)}}{\partial\alpha^n}\right)_\beta = \beta^n \left(\frac{\partial^n Z_0^{(\pm)}}{\partial\beta^n}\right)_\alpha, \tag{2.14}$$

that holds true for bosons [19] as well as for fermions, we can write the specific heat $c_{\rm V}^{(\pm)} = C_{\rm V}^{(\pm)}/N^{(\pm)}$, in units of $k_{\rm B}$, as

$$\frac{c_{\rm V}}{k_{\rm B}} = \beta^2 \frac{\partial^2}{\partial\beta^2} \log Z_0(\beta, \alpha) = \beta^2 \frac{\partial^2}{\partial\beta^2} \log Z_{\rm c}(\beta) + \beta^2 \frac{\partial^2}{\partial\beta^2} \log Z_{\rm d}(\beta) \tag{2.15}$$

(where we have dropped the superscript $(\pm)$ as insignificant in this case). According to Eq. (2.15), the specific heat is just the sum of the heat capacities of the two systems, each of them containing a single particle under canonical conditions, and described by the Hamiltonian $H_{\rm c}$ and $H_{\rm d}$, respectively.

Explicit expressions for $Z_n^{(\pm)}$ and $G_n^{(\pm)}$ can be obtained if we assume that the density of states of the continuous spectrum has the form $\sigma(\epsilon_{\rm c}) = C\epsilon_{\rm c}^s$ (C and s

are constants, such that $C > 0$ and $s > -1$), as it happens in most of the cases [7, 8]. Under this assumption we can write:

$$\begin{array}{rcl} Z_n^{(\pm)} & = & \frac{C}{\beta^{s+1}} \sum_{j=0}^{n} C_n^j \Gamma(s+1+n-j) \\ & & \times \sum_{i=0}^{\infty} n_i (\beta\epsilon_i)^j g_{s+1+n-j}^{(\pm)}(\alpha+\beta\epsilon_i) \\ \text{and} & & \\ G_n^{(\pm)} & = & \frac{C}{\beta^{s+1}} \sum_{j=0}^{n} C_n^j \Gamma(s+1+n-j) \\ & & \times \sum_{i=0}^{\infty} n_i (\beta\epsilon_i)^j g_{s+n-j}^{(\pm)}(\alpha+\beta\epsilon_i)\,, \end{array} \tag{2.16}$$

where n_i is the degeneracy of the level with energy ϵ_i and $C_k^j = n!/j!(n-j)!$. The functions $g_l^{(\pm)}(\alpha)$ are the l^{th} order polylogarithmic functions [14] of argument $e^{-\alpha}$ (bosons) or $-e^{-\alpha}$ (fermions). In the case of ideal particles inside a rectangular box of dimensions $l_x \gg l_y, l_z$, we can write $\epsilon_c = \hbar^2 k_x^2/2m$ and $\epsilon_{\{i,j\}} = \hbar^2(k_{yi}^2 + k_{zj}^2)/2m$, where k_x, k_y, and k_z are the wave vectors along the x, y, and z axes, respectively. The mass of one particle is m and the discrete values of k_{yi} and k_{zj} depend on the boundary conditions. In this case $s = -1/2$. If $l_x, l_y \gg l_z$, then $s = 0$ and $\epsilon_c = \hbar^2(k_x^2 + k_y^2)/2m$, while $\epsilon_i = \hbar^2 k_{zi}^2/2m$. We observe that the function $c_V(T)$ in the crossover region (the region where the BLC happens) is not universal for, say, a given $\sigma(\epsilon_c)$, but it depends on the distribution of the energy levels of H_d. Nevertheless, in all the cases presented in Fig. 2.4, at the onset of the BLC we observe the formation of a maximum, as in the case of MSBEC in restricted geometries. Moreover, in the case of Neumann boundary conditions at the walls of the container, *the maximum is preceded by a minimum* in the BLC from 3D to 2D and from 2D to 1D.

In nanoscopic systems the surface to volume ratio may not be neglijible, hence the boundary conditions may influence their properties, as observed in Section 1.3. In Fig. 2.5 we plot T_{max}/T_c and $c_{V\max}/k_B$ vs. l_3/l, for Dirichlet, Neumann, and periodic boundary conditions, in the cases when $l_1, l_2 \gg l_3$ (Fig. 2.5 (a), (c)) and $l_1 \gg l_2 = l_3$ (Fig. 2.5 (b), (d)). T_c is the bulk BEC temperature, given by the equation $\rho(2\pi\hbar^2/mk_BT_c)^{3/2} = \zeta(3/2)$, ρ is the particle density, ζ is the Riemann zeta function, and $l = \rho^{-1/3}$ is the mean interparticle distance. Since T_{max} converges to a finite value and $T_c \to 0$ when $l_3/l \to 0$, the ratio T_{max}/T_c diverges in this limit. As ρ increases, T_c increases and BLC is gradually replaced by BEC. As a consequence, $\lim_{l_3/l\to\infty} T_{max}/T_c = 1$. Figure 2.5 (c) can make the connection between these numerical calculations and the analytical approximations reported in Ref. [19] (see Fig. 1.7). We can observe that $c_{V\max}$ is higher in Fig. 2.5 (d) than in Fig. 2.5 (c), for each boundary conditions. Nevertheless, the maximum value of $c_{V\max}$, which is about $2.02k_B$, is obtained for periodic boundary conditions in the limit $\rho \to 0$, while at higher densities this decreases below its bulk value, as expected from previous calculations [19].

The study the BLC of ideal particles in harmonic traps is easier since in this situation Z_d can be calculated exactly. If we denote the characteristic frequencies of the harmonic trap by ω_x, ω_y, and ω_z, with $\omega_x \ll \omega_y, \omega_z$, then $Z_c = k_BT/\hbar\omega_x$

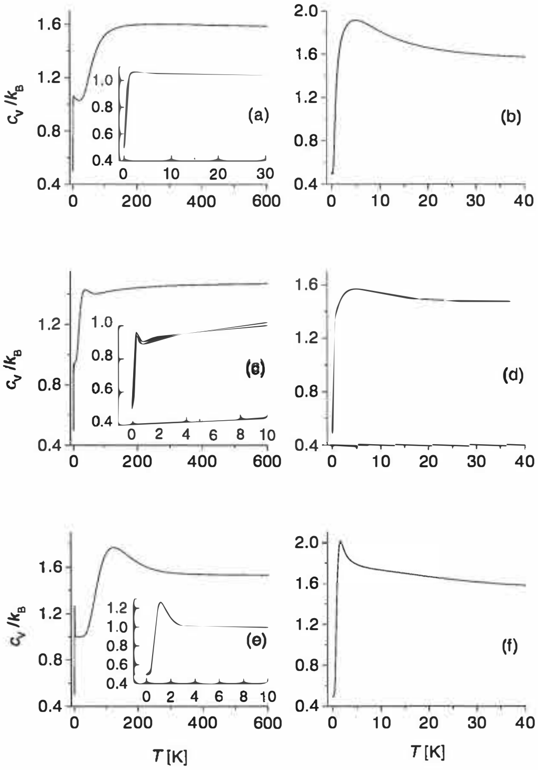

Figure 2.4: Specific heat in units of k_B vs. temperature for ideal Bose and Fermi gases trapped inside cuboidal boxes with Dirichlet ((a) and (b)), Neumann ((c) and (d)), and periodic ((e) and (f)) boundary conditions at the walls. The Figs. (a), (c), and (e) correspond to $l_1 \to \infty$, $l_2 = 10^{-9}$ m, and $l_3 = 10^{-10}$ m, while the Figs. (b), (d), and (f) correspond to $l_1 \to \infty$ and $l_2 = l_3 = 10^{-9}$ m. The particle density is 10^{25} m^{-3} in each case. In each situation the results for bosons (solid line) and fermions (dashed line) are both plotted, but they can not be distinguished. In the insets of (a), (c), and (e) we show low temperature details of the larger graphs (the axes are the same).

and $Z_d = [(1 - \exp(\hbar\omega_x/k_B T))(1 - \exp(\hbar\omega_y/k_B T))]^{-1}$. In this case $dc_V/dT \geq 0$ for any temperature, so BLC is not accompanied by the formation of a maximum. The dimensionality of the system (say, nD) is reflected in the value of c_V, which is nk_B.

2.2 Divergency of the specific heat in systems of fermions

In this section we shall concentrate on Fermi gases close to $T = 0$. We consider again that the Hamiltonian of the system can be approximated by single-particle operators of the form $H = H_c + H_d$, as explained in section 2.1.2. At temperatures

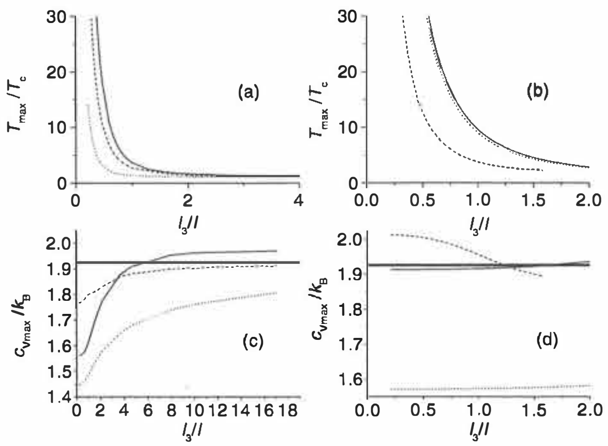

Figure 2.5: The temperature of $c_{V\max}$ of *Bose gases*, scaled by the bulk critical temperature T_c (see the text), as a function of l_3/l (where $l = \rho^{-1/3}$, and ρ is the density), is shown for (a) the membrane geometry ($l_1, l_2 \gg l_3$) and (b) the wire geometry ($l_1 \gg l_2 = l_3$). The value of $c_{V\max}$, in units of k_B, vs. l_3/l, is plotted for (c) membrane geometry and (d) wire geometry (the same as in (a) and (b)). Solid, dashed and dotted lines are used for Dirichlet, periodic and Neumann boundary conditions. The thick horizontal lines in (c) and (d) correspond to the 3D bulk value of c_V at the BEC temperature. In the numerical calculations we varied ρ, keeping $l_3 = 10^{-9}$ m.

close to 0 the chemical potential of a Fermi system approaches the Fermi energy ϵ_F. For $\alpha \ll -1$, the polylogarithmic functions of negative argument can be written in the form [28]:

$$g_n^{(+)}(\alpha) = \frac{|\alpha|^n}{\Gamma(n+1)}\left[1 + \mathcal{O}\left(\frac{1}{\alpha^2}\right)\right]. \qquad (2.17)$$

The case for $n = 1$ is included in (2.17), but can be refined further to write $g_1^{(+)}(\alpha) = |\alpha|\left[1 + \mathcal{O}\left(e^{-\alpha}\right)\right]$. In the other extreme case, when $\alpha \gg 1$, all the polylogarithmic functions have a behavior of the form $g_n^{(\pm)}(\alpha) = e^{-\alpha}\left[1 + \mathcal{O}\left(e^{-\alpha}\right)\right]$. Using these asymptotic expressions we can return to the study of the specific heat close to zero temperature, for a density of energy levels of H_c similar to the one introduced in the previous section, namely $\sigma(\epsilon_c) = C\epsilon_c^s$. The ground state of H_d is nondegenerate since we discuss a finite system. We shall also denote $\alpha_0 \equiv -\beta\epsilon_F$.

A basic result of statistical mechanics is that the chemical potential $\mu \to \epsilon_{\rm F}$ as $T \to 0$. Let us now calculate $\lim_{T\to 0}(|\alpha_0| - |\alpha|)$ when $\epsilon_{\rm F} = \epsilon_i$, $i > 0$ (in all the other cases it will turn out that the limit is zero). Using $N = Z_0^{(+)}(\alpha)$, Eqs. (2.16), and the definition of the Fermi energy, we write two different expressions for the total number of particles in the system:

$$
\begin{aligned}
N &= \frac{C}{(s+1)\beta^{s+1}}\left\{|\alpha|^{s+1} + \ldots + (|\alpha| - \beta\epsilon_{i-1})^{s+1}\right\} \\
&\quad + n_i C\frac{\Gamma(s+1)}{\beta^{s+1}} g_{s+1}^{(+)}(\alpha+\beta\epsilon_i) + \qquad (2.18)\\
&\quad C\frac{\Gamma(s+1)}{\beta^{s+1}} \sum_{j=i+1}^{\infty} n_j e^{|\alpha|-\beta\epsilon_j} \\
&= \frac{C}{(s+1)\beta^{s+1}} \qquad (2.19)\\
&\quad \times \left\{|\alpha_0|^{s+1} + \ldots + (|\alpha_0| - \beta\epsilon_{i-1})^{s+1}\right\} .
\end{aligned}
$$

If we denote $\xi \equiv \alpha + \beta\epsilon_i$, then from (2.18) and (2.19), neglecting the exponentials and assuming that $\lim_{T\to 0}(\xi/|\alpha_0|) = \lim_{T\to 0}(\xi/|\alpha|) = 0$, we obtain, in the case $\alpha_0, \alpha \ll -1$, an equation for ξ:

$$
n_i \frac{g_{s+1}^{(+)}(\xi)}{\xi} = \frac{|\alpha_0|^s}{\Gamma(s+1)}\chi_s\,, \qquad (2.20)
$$

where $\chi_s \equiv 1 + \ldots + n_{i-1}(1-x_{i-1})^s$ and $x_j \equiv \epsilon_j/\epsilon_{\rm F}$. We now notice that we have three distinct situations: (a) $s > 0$, in which case $\xi \to 0$ as $T \to 0$, (b) s=0, and ξ converges to a finite positive value, and (c) $s \in (-1, 0)$, when $\xi \to \infty$ as $T \to 0$.

Let us now analyze the asymptotic behavior of ξ in the case (c), the only case that requires closer investigation. We can write

$$
\frac{e^{-\xi}}{\xi} = \frac{|\alpha_0|^s}{n_i\Gamma(s+1)}\chi_s\,, \qquad (2.21)
$$

so $\xi = (-s)\log|\alpha_0| - \log\xi - \log\left(\chi_s/n_i\Gamma(s+1)\right)$. Therefore, at $\alpha_0 \ll -1$, $\xi \approx |s|\log|\alpha_0| - \log\left[\log|\alpha_0|\right] + \ldots$. We can see now that the assumption $\lim_{T\to 0}(\xi/|\alpha_0|) = \lim_{T\to 0}(\xi/|\alpha|) = 0$ was justified. Also, following the same kind of reasoning, one can prove that when $\epsilon_{\rm F} \neq \epsilon_i$, for any i, then $\lim_{T\to 0}(|\alpha_0| - |\alpha|) = 0$ for any s.

Using Eqs. (2.20) and (2.21) we can calculate the specific heat close to $T = 0$. For that we have to evaluate the functions $G_2^{(+)}$, $G_1^{(+)}$, $G_0^{(+)}$, and $Z_0^{(+)}$. We analyze again the case when $\epsilon_{\rm F} = \epsilon_i$, $i > 0$. After some algebra and dropping out the exponentially small factors, we can write:

$$
G_2^{(+)} = \frac{C|\alpha|^{s+2}}{\beta^{s+1}}\left\{\chi_s + n_i\left[\Gamma(s+3)\frac{g_{s+2}^{(+)}(\xi)}{|\alpha|^{s+2}}\right.\right. \qquad (2.22)
$$

$$+2\Gamma(s+2)y_i\frac{g_{s+1}^{(+)}(\xi)}{|\alpha|^{s+1}}+\Gamma(s+1)y_i^2\frac{g_s^{(+)}(\xi)}{|\alpha|^s}\Bigg]\Bigg\},$$

$$G_1^{(+)} = \frac{C|\alpha|^{s+1}}{\beta^{s+1}}\Bigg\{\chi_s+n_i\Bigg[\Gamma(s+2)\frac{g_{s+1}^{(+)}(\xi)}{|\alpha|^{s+1}} \tag{2.23}$$

$$+\Gamma(s+1)y_i\frac{g_s^{(+)}(\xi)}{|\alpha|^s}\Bigg]\Bigg\},$$

$$G_0^{(+)} = \frac{C|\alpha|^s}{\beta^{s+1}}\left\{\chi_s+n_i\Gamma(s+1)\frac{g_s^{(+)}(\xi)}{|\alpha|^s}\right\}, \tag{2.24}$$

$$Z_0^{(+)} = \frac{C|\alpha|^{s+1}}{(n+1)\beta^{s+1}}\left\{\chi_{s+1}+n_i\Gamma(s+2)\frac{g_{s+1}^{(+)}(\xi)}{|\alpha|^{s+1}}\right\}, \tag{2.25}$$

where $y_j=\beta\epsilon_j/|\alpha|$. To see the asymptotic behavior, we calculate c_V separately for the cases (a), (b), and (c). Using Eqs. (2.20,2.22-2.25) and working consistently in the orders of $|\alpha|$, we obtain the results:

- *Case (a)*

$$\frac{c_V}{k_B} = \frac{(s+1)|\alpha|}{\chi_{s+1}+\Gamma(s+2)n_i g_{s+1}^{(+)}(\xi)/|\alpha|^{s+1}} \times\left\{\frac{n_i^2\Gamma^2(s+1)}{\chi_s}\frac{g_s^{(+)^2}(\xi)}{|\alpha|^{2s}} + \frac{n_i^3\Gamma^3(s+1)}{\chi_s^2}\frac{g_s^{(+)^3}(\xi)}{|\alpha|^{3s}}+\mathcal{O}\left(\frac{1}{|\alpha|^{s+2}}\right)\right\}, \tag{2.26}$$

- *Case (b)*

$$\frac{c_V}{k_B} = \frac{n_i}{|\alpha|\left(\chi_1+n_i g_1^{(+)}(\xi)/|\alpha|\right)} \times\left\{\frac{\chi_0 g_0^{(+)}(\xi)}{\chi_0+n_i g_0^{(+)}(\xi)}\xi^2+\frac{2\chi_0 g_1^{(+)}(\xi)}{\chi_0+n_i g_0^{(+)}(\xi)}\xi +2g_2^{(+)}(\xi)-\frac{n_i g_1^{(+)^2}(\xi)}{\chi_0+n_i g_0^{(+)}(\xi)}\right\}, \tag{2.27}$$

- *Case (c)*

$$\frac{c_V}{k_B} = \frac{s+1}{\chi_{s+1}+n_i\Gamma(s+2)g_{s+1}^{(+)}(\xi)/|\alpha|^{s+1}}\frac{|\alpha|}{\xi} \times\left\{\chi_s+\frac{\chi_s}{\xi}+\mathcal{O}\left(\frac{1}{|\alpha|}\right)\right\}. \tag{2.28}$$

Hence, for $\epsilon_{\rm F} = \epsilon_i$, $i > 0$, from Eqs. (2.26-2.28) we distinguish the following situations:

($a1$) $s > 1/2$, then $c_{\rm V}/k_{\rm B} \propto (\epsilon_{\rm F}/k_{\rm B}T)^{1-2s}$, and $c_{\rm V} \to 0$ as $T \to 0$ (note that if $s > 2$ some of the orders of α interchange, but the function $c_{\rm V}$ converges fast to zero as T approaches 0);

($a2$) $s = 1/2$, then $\lim_{T\to 0}(c_{\rm V}/k_{\rm B}) = (3 - 2\sqrt{2})(3\pi/8)\zeta^2(1/2)n_i^2/\chi_{3/2}\chi_{1/2}$;

($a3$) $s \in (0, 1/2)$, then $c_{\rm V}/k_{\rm B} \propto (\epsilon_{\rm F}/k_{\rm B}T)^{1-2s}$, and $c_{\rm V} \to \infty$ as $T \to 0$;

(b) $s = 0$, then $c_{\rm V}/k_{\rm B} \propto k_{\rm B}T/\epsilon_{\rm F}$, and $c_{\rm V} \to 0$ as $T \to 0$;

(c) $s \in (-1, 0)$, then $c_{\rm V}/k_{\rm B} \propto (\epsilon_{\rm F}/k_{\rm B}T)/\log(\epsilon_{\rm F}/k_{\rm B}T)$, and $c_{\rm V} \to \infty$ as $T \to 0$.

Therefore, in the cases ($a3$) and (c), $c_{\rm V}$ presents a divergent behavior at $T = 0$, while in case ($a2$) it approaches a finite limit. Since these situations are in contradiction with the expected result $\lim_{T\to 0} c_{\rm V} = 0$, we clarify them by noting that this is due to the approximation that the spectrum of $H_{\rm c}$ is continuous. This does not happen in any finite system and therefore, at low enough temperature the specific heat approaches zero, as expected.

Without getting into details we state that when $\epsilon_{\rm F} \neq \epsilon_i$, for any $i \geq 0$, similar calculations lead us to the results $\lim_{T\to 0}(|\alpha_0| - |\alpha|) = 0$ and $\lim_{T\to 0} c_{\rm V} = 0$ for any s. On the other hand, the continuity of μ as a function of $\epsilon_{\rm F}$ implies the continuity of α and $c_{\rm V}$ as functions of $\epsilon_{\rm F}$, for any $T > 0$. In other words, a divergent behavior in the cases ($a3$) and (c) can be approached asymptotically for any $T > 0$, as $\epsilon_{\rm F} \to \epsilon_i$ (for any i), by the functions $c_{\rm V}(T)$. This leads to the formation of a maximum at finite temperature, with the properties: $c_{\rm V max} \to \infty$ and $T_{\rm max} \to 0$, as $\epsilon_{\rm F} \to \epsilon_i$, for all $i > 0$.

Let us now make the connection with familiar systems, namely with the ones discussed in section 2.1.2. In the case of a cuboidal box with dimensions $l_{\rm x} \gg l_{\rm y}, l_{\rm z}$, $s = -1/2$, hence we have the case (c). In Fig. 2.6 we plot the numerical results for such a fermionic system, with dimensions $l_1 \to \infty$, $l_2 = l_3 = 10^{-9}$ m. The mass of the particles is chosen as in section 2.1.2, such that $\lambda^2 = 10^{-18}T^{-1}$ m^{2}K. We observe the formation of a maximum as the Fermi energy approaches the first excited energy level of $H_{\rm c}$, and the divergent behavior at $\epsilon_{\rm F} = \epsilon_1$. If the fermions are inside a cuboidal box with dimensions $l_{\rm x}, l_{\rm y} \gg l_{\rm z}$ or a harmonic potential with the characteristic frequencies $\omega_{\rm x} \ll \omega_{\rm y}, \omega_{\rm z}$, then $s = 0$ and we have case (b), therefore we do not observe the formation of a similar maximum. This was checked by numerical calculations and was found to be correct.

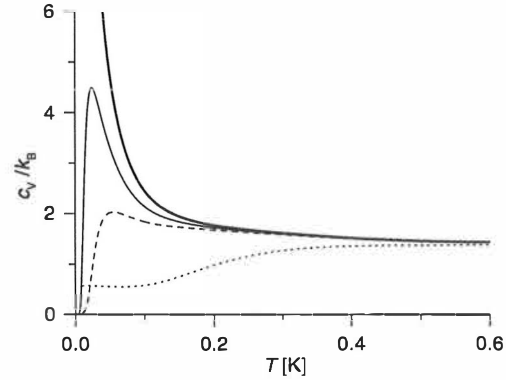

Figure 2.6: The specific heat (in units of k_B) of a Fermi gas trapped inside a cuboidal box ($l_1 \to \infty$, $l_2 = l_3 = 10^{-9}$ m) with Neumann boundary conditions on the walls. The four curves correspond to the following densities: 1.5×10^{26} m^{-3} (dotted line), 9.2×10^{26} m^{-3} (dashed line), 9.6×10^{26} m^{-3} (solid line), and 1×10^{27} m^{-3} (thick solid line). This last case corresponds to $\epsilon_F = \epsilon_1$.

Chapter 3

Nonequilibrium superconductivity: diffusion and trapping of quasiparticles

3.1 Introduction

Normal metal-insulator-superconducting (NIS) junctions can be used in a variety of applications. This chapter is devoted to the cooling properties of such junctions. By placing an insulating layer between a normal metal and a superconductor, one can extract selectively electrons from the normal metal, reducing in this way its temperature. In Fig. 3.1 it is shown schematically how the hot electrons are extracted from the normal metal through one junction and cold electrons are introduced into it through the other junction. The first part of the cooling process is represented by the tunneling phenomenon through the junction, and is discussed in Section 3.2. The second part, analyzed in Section 3.3, concerns the diffusion and trapping of nonequilibrium quasiparticles formed in the superconductor. The general results will be combined in Section 3.4, where the possibility of constructing coolers using NIS junctions is investigated. Analytical approximations will be presented in Section 3.5.

3.2 Tunneling processes in NIS junctions

When a thin insulating material (usually an oxide layer) is placed between a normal metal and a superconductor, forming in this way a NIS junction, the electrical charges can still penetrate from one side to another by tunneling. The thickness of the insulator determines the tunneling probability, which is inversely proportional to the resistance of the junction, R_{T}. The tunneling hamiltonian

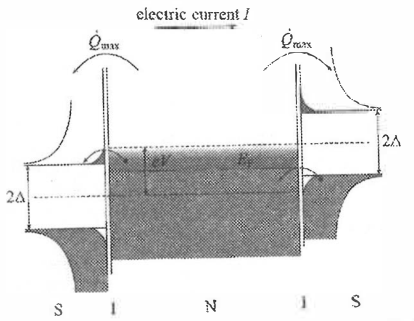

Figure 3.1: The basics of the cooling process, using a pair of NIS junctions. The hot electrons are extracted from the normal metal (N), through the insulating layer (I) on the left, and deposited into the left superconductor (S). On the right hand side, cold electrons are extracted from the superconductor and deposited into the normal metal. All these processes lead to the reduction of the average energy of the electron gas, i. e. reduction of the temperature in the normal metal. The weak coupling between the electrons and the phonons in a metal, at such low temperatures [29], allows the onset of a nonzero temperature difference between these two subsystems in the process.

can be written in the general form [30]:

$$H_T = \sum_{\mathbf{k}_s,\mathbf{k}_n,\sigma} \{T_{\rm sn} c^+_{\mathbf{k}_s,\sigma} c_{\mathbf{k}_n,\sigma} + T^*_{\rm sn} c^+_{\mathbf{k}_n,\sigma} c_{\mathbf{k}_s,\sigma}\},$$

where $T_{\rm sn}$ is the tunneling matrix element, while $c^+_{\mathbf{k}_n,\sigma}$ and $c^+_{\mathbf{k}_s,\sigma}$ are creation operators on the states with momenta $\mathbf{k}_n$ and $\mathbf{k}_s$, respectively, and projection of spin σ. All through this chapter, the superscripts "n" and "s" will refer to normal metal and superconductor, respectively. We also make the assumption that the tunneling yields no spin flips. Using the linear transformation of the electron operators, $c_{\mathbf{k}_s,\sigma}$ and $c^+_{\mathbf{k}_s,\sigma}$, into quasiparticle operators, $\gamma_{\mathbf{k}_s\sigma}$ and $\gamma^+_{\mathbf{k}_s\sigma}$, introduced in Eqs. (1.24) of Section 1.2.2, and the Cooper pair creation and annihilation operators, S^+ and S [31, 32], we can write the terms of the tunneling hamiltonian as in [33]

$$\begin{aligned}
T_{\rm sn} c^+_{\mathbf{k}_s,\sigma} c_{\mathbf{k}_n,\sigma} + T^*_{\rm sn} c^+_{\mathbf{k}_n,\sigma} c_{\mathbf{k}_s,\sigma} &= T_{\rm sn}(u_{\mathbf{k}_s}\gamma^+_{\mathbf{k}_s\sigma} + v^*_{\mathbf{k}_s} S^+ \gamma_{-\mathbf{k}_s-\sigma}) c_{\mathbf{k}_n,\sigma} \\
&\quad + T^*_{\rm sn} c^+_{\mathbf{k}_n,\sigma}(u^*_{\mathbf{k}_s}\gamma_{\mathbf{k}_s\sigma} + v_{\mathbf{k}_s} S \gamma^+_{-\mathbf{k}_s-\sigma}) \\
&= \underbrace{u_{\mathbf{k}_s} T_{\rm sn} \gamma^+_{\mathbf{k}_s\sigma} c_{\mathbf{k}_n,\sigma}}_{j_1} + \underbrace{v^*_{\mathbf{k}_s} T_{\rm sn} S^+ \gamma_{-\mathbf{k}_s-\sigma} c_{\mathbf{k}_n,\sigma}}_{j_4} \\
&\quad + \underbrace{u^*_{\mathbf{k}_s} T^*_{\rm sn} c^+_{\mathbf{k}_n,\sigma}\gamma_{\mathbf{k}_s\sigma}}_{j_3} + \underbrace{v_{\mathbf{k}_s} T^*_{\rm sn} c^+_{\mathbf{k}_n,\sigma} S \gamma^+_{-\mathbf{k}_s-\sigma}}_{j_2},
\end{aligned}$$

where j_1 and j_2 represent the densities in energy of the currents of electrons and holes, respectively, passing from the normal metal into the superconductor, while j_3 and j_4 represent the reverse currents. Expressing the tunneling probability in terms of the normal state tunneling resistance, we obtain the expressions for the four currents, as functions of energy:

$$\begin{aligned} j_1(\epsilon)&=g(\epsilon)f_\mathrm{n}(\epsilon-eV,T_\mathrm{n})[1-f_\mathrm{s}(\epsilon,T_\mathrm{s})]/e^2R_\mathrm{T},\\ j_2(\epsilon)&=g(\epsilon)f_\mathrm{n}(\epsilon+eV,T_\mathrm{n})[1-f_\mathrm{s}(\epsilon,T_\mathrm{s})]/e^2R_\mathrm{T},\\ j_3(\epsilon)&=g(\epsilon)[1-f_\mathrm{n}(\epsilon-eV,T_\mathrm{n})]f_\mathrm{s}(\epsilon,T_\mathrm{s})/e^2R_\mathrm{T},\\ j_4(\epsilon)&=g(\epsilon)[1-f_\mathrm{n}(\epsilon+eV,T_\mathrm{n})]f_\mathrm{s}(\epsilon,T_\mathrm{s})/e^2R_\mathrm{T}, \end{aligned} \tag{3.1}$$

where $f_\mathrm{n,s}(\epsilon, T_\mathrm{n,s})$ represent the populations of the electron (in the normal metal) and quasiparticle (in the superconductor) energy levels, at some effective temperatures T_n and T_s, respectively. V is the voltage across the junction and the electron charge is e. The energy ϵ is measured from the Fermi energy in the superconductor and it is always taken in absolute value. Although $f_\mathrm{n,s}$ may not be Fermi distributions in our case of nonequilibrium [34] we make the assumption that $1 - f_\mathrm{n}(-\epsilon, T_\mathrm{n}) = f_\mathrm{n}(\epsilon, T_\mathrm{n})$, which is an identity for a Fermi distribution, to transform the expressions that involved negative ϵ. In what follows I shall concentrate on the junction where the flux of electrons is oriented from the normal metal into the superconductor (left side in Fig. 3.1), where eV is positive. Using Eqs. (3.1), the particle and excitation fluxes, J_e and J_q, respectively, can be written as

$$J_e = \frac{1}{e}I_e = \int_\Delta^\infty (j_1 - j_2 - j_3 + j_4)\, d\epsilon \tag{3.2}$$
$$= \frac{1}{e^2R_\mathrm{T}}\int_\Delta^\infty g(\epsilon)[f_\mathrm{n}(\epsilon-eV,T_\mathrm{n}) - f_\mathrm{n}(\epsilon+eV,T_\mathrm{n})]\, d\epsilon,$$

$$J_q = \int_\Delta^\infty (j_1 + j_2 - j_3 - j_4)\, d\epsilon \tag{3.3}$$
$$= \frac{1}{e^2R_\mathrm{T}}\int_\Delta^\infty g(\epsilon)[f_\mathrm{n}(\epsilon-eV,T_\mathrm{n}) + f_\mathrm{n}(\epsilon+eV,T_\mathrm{n}) - 2f_\mathrm{s}(\epsilon,T_\mathrm{s})]\, d\epsilon.$$

The power flux transported by the electrons from the normal metal into the superconductor is given by the formula [33]

$$P_e = \int_\Delta^\infty [(\epsilon - eV)(j_1 - j_3) - (\epsilon + eV)(j_4 - j_2)]\, d\epsilon \tag{3.4}$$
$$= \int_\Delta^\infty [\epsilon(j_1 + j_2 - j_3 - j_4) - eV(j_1 - j_2 - j_3 + j_4)]\, d\epsilon.$$

We observe that, while J_e depends only on T_n and is independent of T_s, both J_q and P_e also depend on T_s. As T_s increases, the power extracted from the normal metal decreases, and it turns out that it is important to keep the superconductor at as low temperature as possible, in order to have an efficient cooling of the normal metal. In order to evaluate the temperature of the superconductor, we have to model the diffusion of the quasiparticles into the superconductor. This problem will be discussed in the next section.

3.3 The diffusion of quasiparticles in superconductors

The cooler consists of a very thin film of normal metal, which is to be cooled, in contact, through an oxide layer, with the superconducting film. The widths of the films vary from about 0.3 μm up to 6 μm. In the case of small junctions, the length of the normal metal film is a few microns, while in the case of large junctions, it is 10 to 30 μm. The length of the superconducting film is considered to be infinite. See Paper IV and citations therein for more details about the experimental design.

From the fact that a quasiparticle excitation, say $\gamma^{+}_{q\sigma}|BCS\rangle$, where q and σ correspond to the quasiparticle wave-number and spin, respectively, is an eigenstate of the wave-number operator, with eigenvalue q, and from the dispersion equation, one can deduce the energy dependent quasiparticle group velocity, $v(\epsilon, x) = v_{\mathrm{F}}\sqrt{1-(\Delta(x)/\epsilon)^2}$. The Fermi velocity is denoted by v_{F} [35, 36]. The diffusion constant $D(\epsilon, x) \equiv (1/2)v(\epsilon, x)a$, where a is the elastic mean free path, follows immediately: $D(\epsilon, x) = (v(\epsilon, x)/v_F)D_{\mathrm{n}}$ [36]. Here $D_{\mathrm{n}} = (\rho_{\mathrm{n}}e^2\sigma(\epsilon_{\mathrm{F}}))^{-1}$ is the *normal diffusion constant* of the superconducting film, determined by extrapolating the resistivity ρ_{n} of its normal state towards zero temperature. Since in the cooling experiments the quasiparticle energies lie close to the gap energy, the diffusion constant is very small. Moreover, the excess population of the quasiparticle levels could decrease the energy gap in the junction region, lowering in this way the cooling performance. As a consequence of this, it was observed in the experiment that if bare superconducting films were used in the construction of the coolers, no appreciable reduction in temperature takes place in the normal metal island (see Paper IV). Therefore, the quasiparticles should be driven away from the junction regions.

In Paper IV we show how one can remove the excess quasiparticle excitations from the regions near the junctions by attaching a semi-infinite normal metal electrode to the superconductor, forming in this way a bilayer structure, which acts as a "trap" for injected hot quasiparticles. To calculate the quasiparticle flux we have to write down the diffusion equation. In all the situations discussed here a film of Cu was used as the normal metal, while the superconducting metal was Al.

Let us consider the NIS structure presented in Fig. 3.2 (b) (all the geometrical notations will refer to this figure), where the electrons pass from the normal metal into the superconductor. The other junction of the SINIS structure (S, I, and N denote the superconductor, insulator, and normal metal, respectively) can be treated in a similar manner. By $\Delta(x)$ we denote the nonconstant energy gap of the superconductor. We take the gap energy in a bare Al film to be $\Delta_0 = 200$ μeV, and deep in the bilayer region $\Delta_{\mathrm{N}} < \Delta_0$ because of the proximity effect, in the case of direct metal-to-metal contact between Cu and Al. The

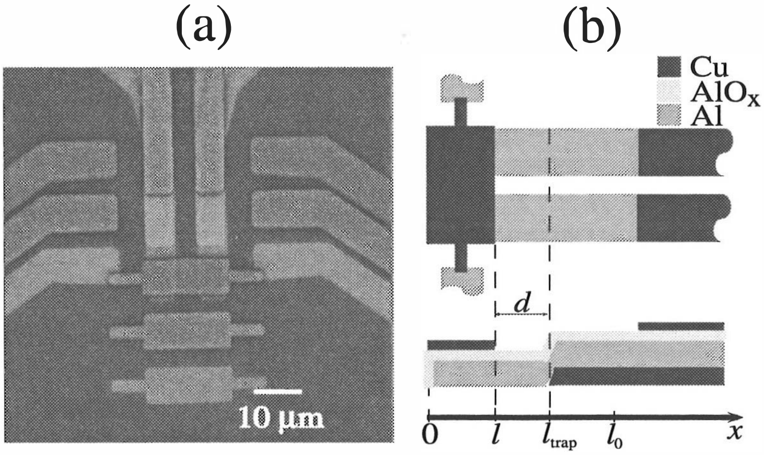

Figure 3.2: The SEM image **(a)** of a large SINIS cooler used in Paper IV, with junction area $\geq 10\ \mu\text{m}^2$ and its schematic illustration **(b)** from above (up) and in cross-section (down). The cooling junction is in the range $[0, l]$, while the bilayer trap starts at the distance l_{trap} from the origin. The parameter l_0 is defined such that $\Delta(x) = \Delta_{\text{N}}$ for $x \geq l_0$ .The thick line on top of the Al film ((b) down) represents the oxide layer and forms the junction in the range $[0, l]$.

excess quasiparticles in the junction region can disappear or change their energy mainly by one of the following processes: interaction with each other, diffusion, recombination, inelastic scattering on the lattice, and tunneling back into the normal metal. All the last three phenomena heat the normal electrode. A monotonic decrease of the energy gap outside of the junction area would enhance the outgoing quasiparticle flux because of the increase of the diffusion constant and of the probability of quasiparticle relaxation by inelastic collisions with the lattice, outside the junction region. A quasiparticle trap through an oxide barrier, similar and close to the junction could be useful in small area (SI)NIS structures, since this would decrease the population of the quasiparticle levels by tunneling into the normal trap. Taking into account all these effects, we can write the diffusion equation for the population of the quasiparticle energy levels in an interval $[\epsilon, \epsilon + d\epsilon)$ at point x, in the approximation that all the processes are local. Then, if we consider that the quasiparticle distribution at point x can be approximated by the thermal Fermi distribution $f(\epsilon, T_{\text{s}}(x))$ corresponding to temperature $T_{\text{s}}(x)$ (usually we have $T_{\text{s}} > T_{\text{b}} > T_{\text{n}}$, where T_{b} is the heat bath temperature and T_{n} is the temperature of the electrons in the normal electrode), and integrate over all

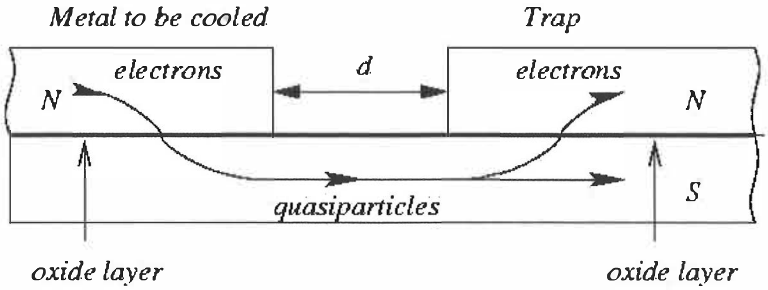

Figure 3.3: Schematic drawing of the electrons and quasiparticles flow in a cooler with a trap in contact with the superconductor through an oxide layer.

energies, we obtain a second order nonlinear differential equation for $T_s(x)$:

$$\begin{aligned}
&\left(\frac{d^2T_s}{dx^2}\right)\int_{\Delta(x)}^{\infty} n_0 D_n \left.\frac{\partial f(\epsilon,T_s)}{\partial T_s}\right|_x d\epsilon + \left(\frac{dT_s}{dx}\right)^2 \int_{\Delta(x)}^{\infty} n_0 D_n \left.\frac{\partial^2 f(\epsilon,T_s)}{\partial T_s^2}\right|_x d\epsilon \\
&-\left(\frac{dT_s}{dx}\right) n_0 D_n \frac{d\Delta(x)}{dx} \left.\frac{\partial f(\Delta,T_s)}{dT_s}\right|_x \\
&-[\Upsilon_{\mathrm{rec}}(T_s,x) - \Upsilon_{\mathrm{gen}}(T_b,x)] - (\Upsilon_{\mathrm{ph}} - \Upsilon_{\mathrm{excit}}) \\
&+\int_{\Delta(x)}^{\infty} j_q(V,\epsilon,T_n,T_s(x),x)d\epsilon + \int_{\Delta(x)}^{\infty} j_q'(0,\epsilon,T_s,T_b,x)d\epsilon = 0.
\end{aligned} \tag{3.5}$$

The constant $n_0 = w_s d_s(\sqrt{2m^3}/\pi^2\hbar^3)\sqrt{\epsilon_F}$ is the density of electron states at Fermi energy ϵ_F, per unit length, along Ox axis. The terms $\Upsilon_{\mathrm{rec}} = w_s d_s R n^2(T_s, x)$ [33, 36] and $\Upsilon_{\mathrm{gen}} = \Upsilon_{\mathrm{rec}}(T_b, x)$ account for the quasiparticle recombination and thermal generation rates, respectively. R is the recombination constant and $n(T,x)$ is the quasiparticle density at temperature T and at position x. $(\Upsilon_{\mathrm{ph}} - \Upsilon_{\mathrm{excit}})$ accounts for the inelastic interaction of quasiparticles with phonons and $j_q(V,\epsilon,T_n,T_s(x),x)$ is the density of the excitation current of energy ϵ through the unit length of the junction, at position x [33]. Therefore note that, formally, $\int_{\Delta(x)}^{\infty} j_q(V,\epsilon,T_n,T_s,x)d\epsilon = J_q(V,T_n,T_s)/l$, where l is the length of the junction. U is the voltage across the junction and $j_q = 0$ for $x > l$. In the case of a trap attached to the superconductor through an oxide barrier $j_q'(0,\epsilon,T_s,T_b,x)$ represents the term corresponding to the tunneling of quasiparticles into the trap. In the present case the oxide layer in the trap region is identical to the one that forms the junction, $j_q'(0,\epsilon,T_s,T_b,x \geq l_{\mathrm{trap}}) = j_q(0,\epsilon,T_s,T_b,x \leq l)$ (see Fig. 3.3). In all the other cases $j_q' \equiv 0$. The expansion of the quasiparticle phase-space in the bilayer region for the case of trap in metal-to-metal contact was not taken into account in Eq. (3.5). In the absence of a rigourous microscopical theory for the density of states in this situation, this can be incorporated by changing the energy gap (Fig. 3.4).

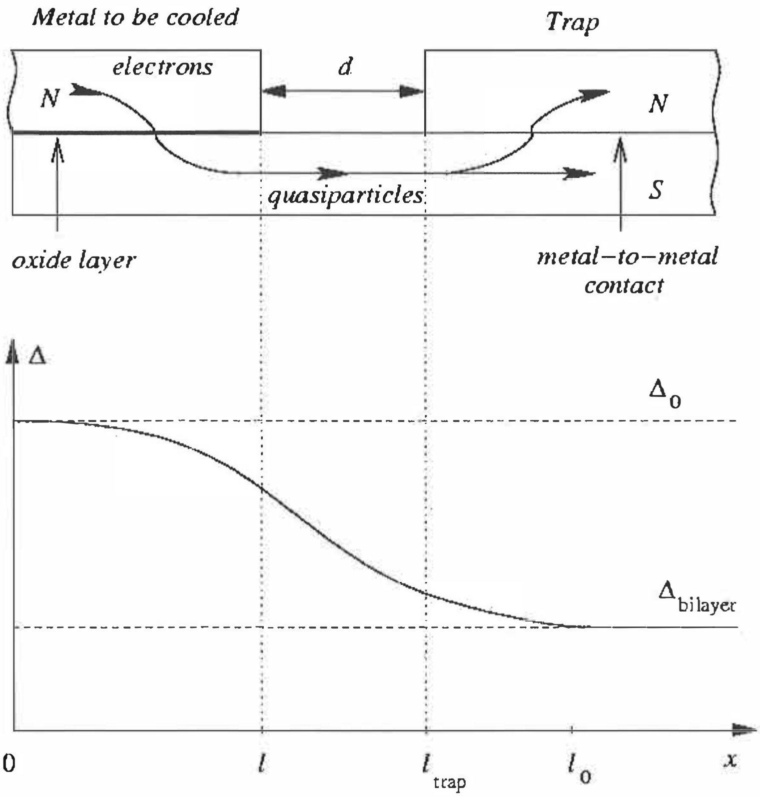

Figure 3.4: **Top:** schematic drawing of the electrons and quasiparticles flow in a cooler with a trap in metal-to-metal contact with the superconductor. **Bottom:** the variation in space of the energy gap.

3.4 Coolers

To calculate the temperature of the electron gas in the normal metal we have to equate the heat flow to zero. If we neglect the heat dissipated by the electrical current into the normal metal, the equation obtained is

$$\begin{aligned} &\textstyle\int_0^l dx \left\{\int_{\Delta(x)}^{\infty} \epsilon j_{\mathrm{q}}(U, \epsilon, T_{\mathrm{n}}, T_{\mathrm{s}}(x), x), d\epsilon \right. \\ &-k w_{\mathrm{s}} d_{\mathrm{s}} \Delta(x) [\Upsilon_{\mathrm{rec}}(T_{\mathrm{s}}, x) - \\ &\left. \Upsilon_{\mathrm{gen}}(T_{\mathrm{b}}, x)]\right\} - UI - P_{\mathrm{e,ph}} = 0, \end{aligned} \tag{3.6}$$

where $P_{\mathrm{e,ph}} = \Sigma w_{\mathrm{n}} d_{\mathrm{n}} l (T_{\mathrm{b}}^5 - T_{\mathrm{n}}^5)$. Σ is the electron-phonon coupling constant [29], while w_{n}, d_{n}, and l are the dimensions of the normal electrode. For copper $\Sigma \approx 4$ nW/K^5 μm^3 [38]. The fraction of the excess recombination phonon energy

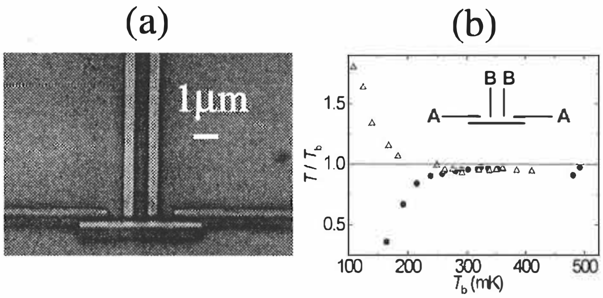

Figure 3.5: **(a)** A SEM image of a basic SINIS cooler with small junctions, schematically shown as an inset in (b). **(b)** Cooling performance of the sample in (a). Horizontal axis gives the bath temperature. Vertical axis shows the temperature of the normal metal at the optimum cooling bias. The two data sets correspond to: pair B as cooler and pair A thermometer (circles), and pair A as cooler and pair B as thermometer (triangles).

absorbed by the electrons in the normal metal is k, while I is the total current through the junction, expressed in terms of T_n, T_s, U, and $\Delta(x)$ [33]. In cooling experiments the quasiparticle energies lie very close to the gap energy, therefore we can neglect the contribution of the inelastic interaction of the quasiparticles with phonons.

Figure 3.5 (a) shows a test sample where two types of low power SINIS coolers (S = aluminium of 18 nm thickness, I = aluminium oxide, N = copper of 28 nm thickness) can operate on the same normal metal electrode. The two pairs of junctions, one at the ends of the central normal metal (copper) island (pair A), and another one in the center (pair B), with superconducting electrodes pointing perpendicularly to the normal metal island, can alternatively be used, one as a SINIS cooling pair and the other one as a SINIS thermometer. The junctions have different sizes between the pairs (ca. 1×0.3 μm^2 with total resistance of 12.5 kΩ in A, and ca. 0.4×0.3 μm^2 with 34.4 kΩ in B), but more importantly, the superconducting aluminium outside the junctions is covered by a film of copper through the same oxide layer as in the tunnel junctions, differently in the two pairs. In pair B the coverage extends from a distance of about 0.2 μm essentially to infinity, in pair A the similar overlap starts only at a distance of 8 μm. Figure 3.5 (b) shows the corresponding cooling performances. It is obvious that pair B works better as a cooler. This illustrative data shows that the cooling characteristics depend on the position of the trap and on the geometry of the junction. Yet, as it will turn out below, the trap with an oxide layer between the normal metal and the superconductor is not sufficiently effective for large junctions.

To investigate the efficiency of a normal metal quasiparticle trap, let us ana-

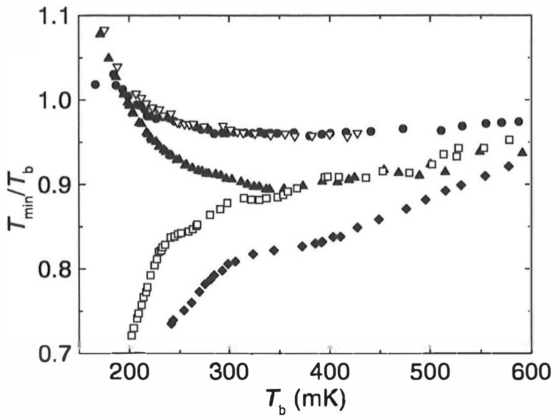

Figure 3.6: Performance of large junction SINIS coolers. T_b on the horizontal axis is the starting temperature, and T_{min} is the temperature of the normal electrode at the optimum bias for cooling. The five samples are otherwise similar, but the differing parameters are such that: filled circles - no quasiparticle trap connected, $2R_T \simeq 630\ \Omega$; down triangles - quasiparticle trap through an oxide layer at $d = 1\ \mu$m, $2R_T \simeq 280\ \Omega$; up triangles - quasiparticle trap in metal-to-metal contact at $d = 5\ \mu$m, $2R_T \simeq 70\ \Omega$; open squares - quasiparticle trap in metal-to-metal contact at $d = 1\ \mu$m, $2R_T \simeq 230\ \Omega$; filled diamonds - quasiparticle trap in metal-to-metal contact at $d = 1\ \mu$m, $2R_T \simeq 50\ \Omega$. The film thickness of the copper trap, aluminium and the normal metal island was 30 nm, 25 nm and 35 nm, respectively.

lyze different SINIS coolers of nominally 4 - 6 μm $\times$ 4 - 6 μm overlap area of the NIS junctions. One should note that this area is typically two orders of magnitude larger than in the conventional electron beam fabricated junctions. Figure 3.6 presents the results obtained in Paper IV. We show the maximum temperature drop for five different samples of large SINIS cooler junctions. One cannot compare the performance of different samples quantitatively from the main figure directly, because the junction resistance (R_T) varies from sample to sample. Clear qualitative conclusions can, however, be made, especially based on the low temperature behavior. The sample with no quasiparticle trap (filled circles), the one with the trap at a distance $d = 1\ \mu$m, but with an aluminium oxide layer between the two metals forming the bilayer (open down-triangles), and the one with the trap in metal-to-metal contact at $d = 5\ \mu$m (filled up-triangles) tend to heat up at $T \lesssim 200$ mK. The sample shown with open up-triangles had a similar oxide layer between the superconductor and the copper layers to what was used to form the oxide barrier in the (SI)NIS junctions. In the two remaining samples, the one shown with open squares and the one with filled diamonds, the copper-

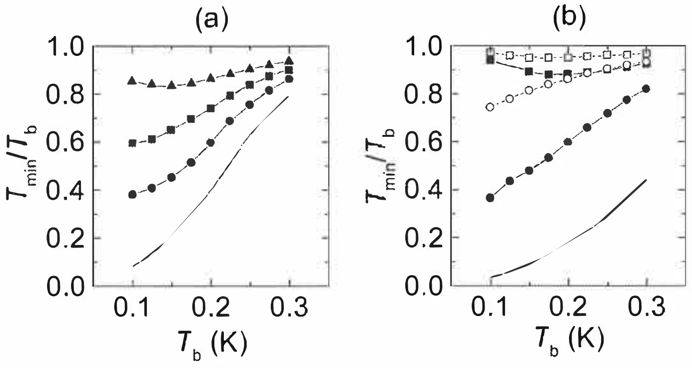

Figure 3.7: Theoretical results of the minimum temperature of the normal metal, normalized to the bath temperature, vs. bath temperature, for large junctions (the area of one junction is 4×4 μm^2), in the following situations (see Fig. 3.6 for the corresponding experimental results): **(a)** $R_T = 110$ Ω and $d = 1$ (circles), 5 (squares) and 10 μm (up triangles). $\Delta_N/\Delta_0 = 1/3$; **(b)** $R_T = 30$ Ω, $\Delta_N/\Delta_0 = 1/3$, and $d = 1$ (filled circles) and 5 μm (filled squares) . For comparison we show the corresponding results for $\Delta_N/\Delta_0 = 1/2$, with open circles and squares. The simple solid lines show the cooling results at optimum bias voltage in the ideal cases when $T_s(x) = T_b$ and $\Delta(x) = \Delta_0$ for all x.

to-aluminium direct metal-to-metal contact is at a distance of less than 1 μm. One can see that in each case the cooling performance is superior down to 200 mK and beyond. The difference in performance between these two samples can be explained qualitatively by the difference of R_T in them. A separate control measurement of a sample with two different values of d from the same fabrication batch were also performed to confirm the conclusion.

We will now briefly outline the theoretical calculations. Since $\Delta(x)$ should depend on the geometry and on $T_s(x)$, one can find all the information regarding the cooling effect by solving Eqs. (3.5) and (3.6) self-consistently. Proper boundary conditions for Eq. (3.5) would be $\partial T_s/\partial x = 0$, at $x = 0$ (zero diffusion current), and $T_s = T_b$ at $x \to \infty$. In the case of a trap in direct metal-to-metal contact we approximate $\Delta(x)$, in the range $0 \leq x \leq l_0$, by the solution of the Ginzburg-Landau equation: $\Delta(x) = -\Delta_0 \tanh\left[(x - (l_0 + y_0))/(\sqrt{2}\xi)\right]$. The parameter y_0 is calculated such that $\Delta(x \geq l_0) = \Delta_N$. We used $R = 26$ μm^{3}s^{-1}, from Ref. [36], and D_n, for large junctions, was calculated to be 140 cm^{2}s^{-1}, from our measured resistivity of the normal Al film, at 4.2 K. Choosing $\xi = 1$ μm and $l_0 - l_{trap} = 0.5$ μm (detailed microscopic calculations should give better approximations for these parameters) we calculated the minimum temperature of the electron gas in the normal electrode of the large NIS junction, as a function of

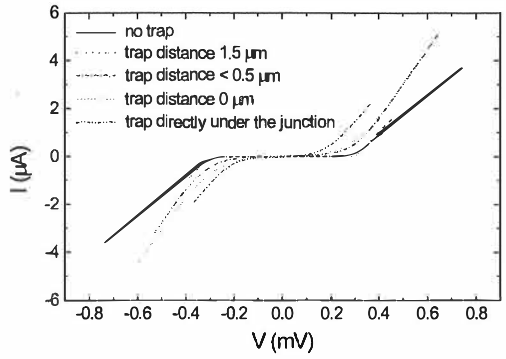

Figure 3.8: Experimental IV-curves for the configuration with the trap in metal-to-metal contact positioned at the distances indicated in the legend.

T_b. From the experimental IV-curves with different trap positions shown in Fig. 3.8 we conclude that Δ_N/Δ_0 is between 1/3 and 1/2 for our experimental configuration with trap in metal-to-metal contact. We used these two extreme values in our calculations. The results for the configuration with the trap in metal-to-metal contact positioned at the distances $d = 1$, 5 and 10 μm are shown in Fig. 3.7. Although the cooling performance varies with parameters like the resistance of the junctions (R_T), diffusivity (D_n) and the function $\Delta(x)$, clear conclusions can be drawn: a trap positioned close to the junction radically improves cooling at low temperatures.

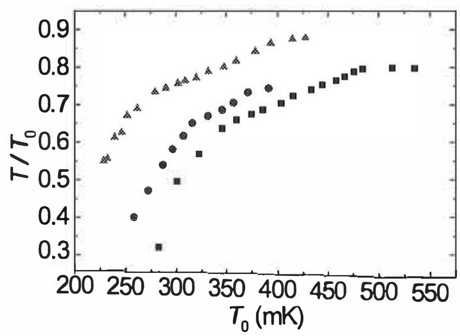

Figure 3.9: Different cooling performances of large junction SINIS structures. An example of an experimental configuration is shown in Fig. 3.10. The aspect ratio of the junction is important for the cooling performance, since a smaller l reduces the probability of back tunneling of excitations into the normal metal island [39].

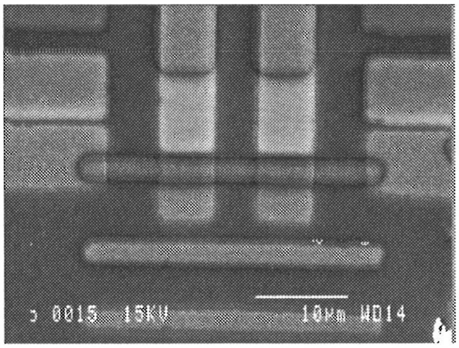

Figure 3.10: Example of experimental setup. The cooling performances of this type of refrigerators are shown in Fig. 3.9 [39].

In recent experiments with large junction SINIS structures, the ratio $T_{\mathrm{min}}/T_{\mathrm{b}}$ was reduced down to 0.3 at temperatures around 300 mK, with a cooling power of about 20 pW (see Fig. 3.9) [39]. The experimental setup is shown in Fig. 3.10.

Direct numerical calculations and our analytical evaluations show that if there is no trap at all (through oxide barrier or in metal-to-metal contact), neither small nor large junctions can work as refrigerators at low temperatures. The small NIS junctions (as in Fig. 3.5), with a trap through the oxide barrier positioned close to it, work efficiently as a cooler, while in the case of large NIS junctions, the thermalization of the superconductor is poor at low temperatures, as observed in the experiment. The theoretical results are shown in Fig. 3.11.

As a conclusion, we have demonstrated that the excess quasiparticle population, i.e. the heating up of a superconductor, can be significantly reduced by drawing the hot quasiparticles from the junction region into a bilayer trap. The performance of such a trap is superior even with moderately large power levels, when the trap is in direct metal-to-metal contact at a short (< 1 μm) distance from the junction injecting heat (the choice of this distance depends mainly on ξ). In smaller junctions, a trap in contact through an oxide barrier seems sufficient for the purpose. We have modeled the heat balance and flow in the (SI)NIS - quasiparticle trap systems. The theoretical calculations explain the observed phenomena.

3.5 Analytical approximations

In the most general case the equations presented in the previous sections of this chapter must be solved numerically . Beside the facts that the numerical calculations are time consuming, and that Eq. (3.5) poses some numerical problems,

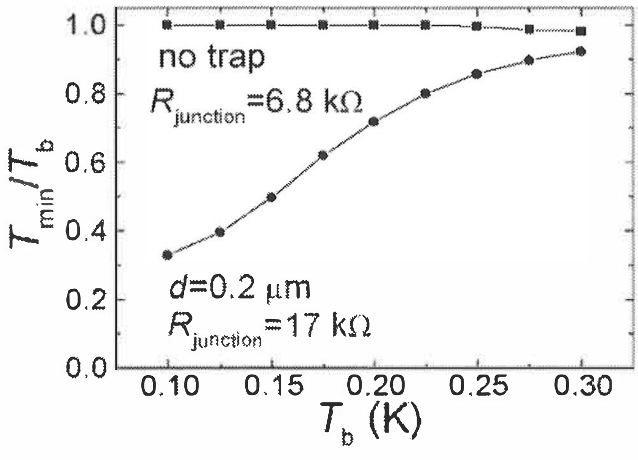

Figure 3.11: Theoretical calculations of the minimum temperature of the electron gas in the normal metal of a cooler with small junctions. The junction parameters, as it is shown on the figure, correspond to the pairs AA and BB of junctions in Fig. 3.5.

it is not easy to draw conclusions of a general nature from such numerical solutions. Fortunately, when the normal metal and the superconductor are at low temperatures, we can find analytical approximations for the formulae introduced.

3.5.1 The cooling power

Let us first take a look at the expression of the heat extracted from the normal electrode through the NIS junction. Using Eqs. (3.1), (3.4), and (3.6), we can write

$$\begin{aligned} P_e &= \frac{1}{e^2 R_{\mathrm{T}} l} \int_0^l dx \int_{\Delta(x)}^{\infty} d\epsilon\, g(\epsilon, \Delta(x))[(\epsilon - eV) f(\epsilon - eV, T_{\mathrm{n}}) \\ &\quad + (\epsilon + eV) f(\epsilon + eV, T_{\mathrm{n}}) - 2\epsilon f(\epsilon, T_{\mathrm{s}}(x))] \\ &\equiv \int_0^l dx\, [j_{\mathrm{p},1}(V,x) + j_{\mathrm{p},2}(V,x) - j_{\mathrm{p},3}(x)] \\ &\equiv J_{\mathrm{p},1}(V) + J_{\mathrm{p},2}(V) - J_{\mathrm{p},3}\,, \end{aligned} \tag{3.7}$$

where we introduced some obvious notations. To calculate $j_{\mathrm{p},1}(V,x)$, $j_{\mathrm{p},2}(V,x)$, and $j_{\mathrm{p},3}(V,x)$, we change the variable of integration, from ϵ to $y = \epsilon - \Delta(x)$. In this way we obtain

$$
\begin{aligned}
j_{\mathrm{p},1}(V,x) &= \frac{1}{e^2 R_{\mathrm{T}} l}\int_{\Delta(x)}^{\infty} d\epsilon \frac{\epsilon}{\sqrt{\epsilon^2-\Delta^2(x)}}(\epsilon - eV) f(\epsilon - eV, T_{\mathrm{n}}) \\
&= \frac{1}{e^2 R_{\mathrm{T}} l}\left\{\int_0^{\infty} dy \sqrt{\frac{y}{y+2\Delta(x)}}\frac{y+\delta}{\exp\left[\beta_{\mathrm{n}}(y+\delta(x))\right]+1}\right. \\
&\quad \left. +\int_0^{\infty} dy \frac{\Delta(x)}{\sqrt{y(y+2\Delta(x))}}\frac{y+\delta}{\exp\left[\beta_{\mathrm{n}}(y+\delta(x))\right]+1}\right\},
\end{aligned}
$$

where $\delta(x) = \Delta(x) - eV$. As usual, $\beta_{\mathrm{n}} = 1/k_{\mathrm{B}}T_{\mathrm{n}}$. Since $\beta_{\mathrm{n}} \gg 1$, the integrand decreases very rapidly with y, due to the exponential function at the denominator. Using the power expansion of $1/\sqrt{1+\tau}$ around $\tau = 0$ and working consistently in the highest and second highest order in the parameter $A_{\mathrm{n}}(x) \equiv \beta_{\mathrm{n}}\Delta(x)$, we can write

$$
\begin{aligned}
j_{\mathrm{p},1}(V,x) &\approx \frac{1}{e^2 R_{\mathrm{T}} l}\frac{1}{\sqrt{2\Delta(x)}}\left\{\Delta(x)\left[\int_0^{\infty} dy \frac{y^{1/2}}{\exp\left[\beta_{\mathrm{n}}(y+\delta(x))\right]+1}\right.\right. \\
&\quad \left. +\delta(x)\int_0^{\infty} dy \frac{y^{-1/2}}{\exp\left[\beta_{\mathrm{n}}(y+\delta(x))\right]+1}\right] \\
&\quad +\frac{3}{4}\left[\int_0^{\infty} dy \frac{y^{3}}{\exp\left[\beta_{\mathrm{n}}(y+\delta(x))\right]+1}\right. \\
&\quad \left.\left. +\delta(x)\int_0^{\infty} dy \frac{y^{1/2}}{\exp\left[\beta_{\mathrm{n}}(y+\delta(x))\right]+1}\right]\right\} \\
&\equiv \frac{1}{e^2 R_{\mathrm{T}} l}\frac{(k_{\mathrm{B}}T_{\mathrm{n}})^2}{\sqrt{2A_{\mathrm{n}}(x)}}\left[A_{\mathrm{n}}(x)\Gamma(3/2) g_{3/2}^{(+)}(a_{\mathrm{n}}(x))\right. \\
&\quad +a_{\mathrm{n}}(x)A_{\mathrm{n}}(x)\Gamma(1/2) g_{1/2}^{(+)}(a_{\mathrm{n}}(x))+ \\
&\quad \left.\frac{3}{4}\Gamma(5/2) g_{5/2}^{(+)}(a_{\mathrm{n}}(x)) + \frac{3}{4}a_{\mathrm{n}}(x)\Gamma(3/2) g_{3/2}^{(+)}(a_{\mathrm{n}}(x))\right],
\end{aligned}
\tag{3.8}
$$

where the polylogarithmic functions $g_l^{(+)}(a)$ have been defined in Section 2.1.2. In a similar manner, if we denote $B_{\mathrm{n}}(x) = \beta_n[\Delta(x) + eV]$ and $A_{\mathrm{s}}(x) \equiv \beta_{\mathrm{s}}\Delta(x)$, we obtain

$$
\begin{aligned}
j_{\mathrm{p},2}(V,x) &\approx \frac{1}{e^2 R_{\mathrm{T}} l}\frac{(k_{\mathrm{B}}T_{\mathrm{n}})^2}{\sqrt{2A_{\mathrm{n}}(x)}}\left[A_{\mathrm{n}}(x)B_{\mathrm{n}}(x)\Gamma\left(\frac{1}{2}\right) g_{1/2}^{(+)}(B_{\mathrm{n}}(x))\right. \\
&\quad \left. +\frac{3}{4}B_{\mathrm{n}}(x)\Gamma(3/2) g_{3/2}^{(+)}(B_{\mathrm{n}}(x))\right]
\end{aligned}
\tag{3.9}
$$

and

$$
j_{\mathrm{p},3}(x) \approx \frac{2}{e^2 R_{\mathrm{T}} l}\frac{(k_{\mathrm{B}}T_{\mathrm{s}})^2}{\sqrt{2A_{\mathrm{s}}(x)}}\left[A_{\mathrm{s}}^2(x)\Gamma\left(\frac{1}{2}\right) g_{1/2}^{(+)}(A_{\mathrm{s}}(x))\right.
$$

$$+\frac{3}{4}A_s(x)\Gamma(3/2)g^{(+)}_{3/2}(A_s(x))\Big] \,. \tag{3.10}$$

In the previous calculations we used $\Delta_0 = 200$ μeV. To see the orders of magnitude of our parameters, let us take $T_n \approx 0.1$ K and $T_b \approx 0.3$ K. In such a case $A_{n,0} \equiv \beta_n\Delta_0 \approx 23$. If $T_s \approx 0.4$ K in the junction region, then $A_{s,0} \equiv \beta_s\Delta_0 \approx 6$. Then it is suitable to make the approximations $g^{(+)}_l(A_{n,0}) \approx e^{-A_{n,0}}$, $g^{(+)}_l(B_{n,0} \equiv \beta_n(\Delta_0 + eV)) \approx e^{-B_{n,0}}$, and $g^{(+)}_l(A_{s,0}) \approx e^{-A_{s,0}}$, for any l.

In cooling experiments we are interested in knowing the optimum cooling power and the optimum bias voltage. If we assume that T_s is independent of V, then $J_{p,3}$ does not influence the result. To simplify the calculations even further, we take a constant energy gap $\Delta(x) = \Delta_0$ in the junction region. Since $J_{p,3}$ is of the order of $B_{n,0}e^{-B_{n,0}}$, as compared to $J_{p,1}$, we can neglect it. We are interested in the low T_n range, so let us write the power extracted from the normal metal in the highest order approximation,

$$\begin{aligned} P_e &= \frac{(k_BT_n)^2}{e^2R_T}\sqrt{\frac{\pi A_{n,0}}{2}}\left[\frac{1}{2}g^{(+)}_{3/2}(a_{n,0}) + a_{n,0}g^{(+)}_{1/2}(a_{n,0})\right] \\ &\quad - J_{p,3}(A_{s,0}). \end{aligned} \tag{3.11}$$

We observe from here directly that for fixed $a_{n,0}$, $P_e \propto T_n^{3/2}$ [40]. An approximation of the optimum bias voltage, $V_{max,0} \equiv (\Delta_0 - \delta_{max,0})/e$, can be calculated by equating to zero the derivative of the power flux, written in the form of Eq. (3.11) with respect to δ_0. Using the general property $dg^{(\pm)}_l(a)/da = -g^{(\pm)}_{l-1}(a)$, we obtain

$$\begin{aligned} \left.\frac{dP_e}{d\delta_0}\right|_{\delta_0=\delta_{max,0}} &= \frac{k_BT_n}{e^2R_T}\sqrt{\frac{\pi A_{n,0}}{2}}\left[\frac{1}{2}g^{(+)}_{1/2}(a_{max,0}) - a_{max,0}g^{(+)}_{-1/2}(a_{max,0})\right] \\ &= 0\,. \end{aligned} \tag{3.12}$$

The solution of Eq. (3.12) is

$$a_{max,0} \equiv \beta_n\delta_{max,0} \approx 0.66\,. \tag{3.13}$$

The optimum cooling power follows immediately:

$$P_{max,0} \approx 0.59\frac{\Delta_0^2}{e^2R_T}\left(\frac{k_BT_n}{\Delta_0}\right)^{3/2} - J_{p,3}(A_{s,0}). \tag{3.14}$$

To see how good this approximation is, we plot in Fig. 3.12 the ratio between the exact value of $a_{n,0}$ at optimum bias, a_{max}, and the approximative value, $a_{max,0}$, given in Eq. (3.13), as a function of $A_{n,0}$. We see that in the range of interest for applications ($A_{n,0} \geq 20$), the accuracy is 95% or higher.

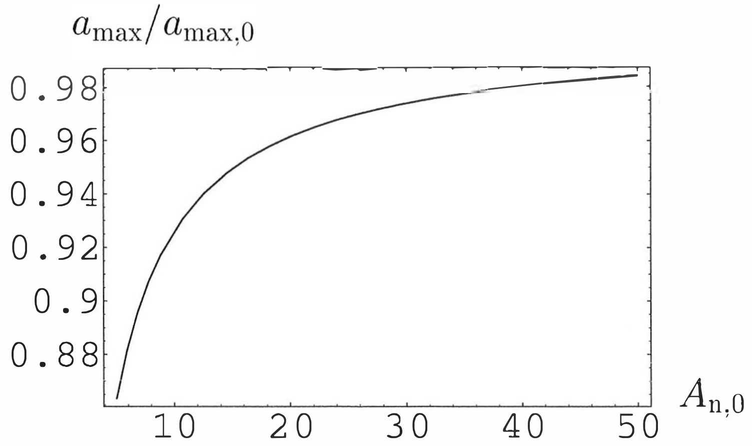

Figure 3.12: The ratio between the exact value of $a_{n,0}$ at the optimum bias, a_{max}, and the solution of Eq. (3.11), $a_{max,0}$, as a function of $A_{n,0}$. Note that a range interesting for applications would be $A_{n,0} \geq 20$.

3.5.2 The diffusion equation

From now on we shall assume that $\Delta(x) = \Delta_0$ for all x, unless otherwise specified. In other words, either we have a trap attached to the superconductor through an oxide layer, or no trap was deposited. In this situation, if we can make the approximation $\beta_s\Delta_0 \approx (\beta_s\Delta_0 + 1)$, the diffusion equation (3.5) can be written in the form:

$$\begin{aligned} k_B T_s n_0 D_n \frac{d^2}{dx^2} y(x) - [\Upsilon_{rec}(T_s, x) - \Upsilon_{gen}(T_b, x)] & \qquad (3.15) \\ + \int_{\Delta(x)}^{\infty} j_q(U, \epsilon, T_n, T_s(x), x) d\epsilon + \int_{\Delta(x)}^{\infty} j'_q(0, \epsilon, T_s, T_b, x) d\epsilon &= 0 , \end{aligned}$$

where

$$y(x) \equiv \beta_s \int_{\Delta_0}^{\infty} f(\epsilon, T_s)\, d\epsilon = g_1^{(+)}(A_{s,0}) \approx e^{-\beta_s\Delta_0} . \qquad (3.16)$$

The terms corresponding to the inelastic scattering of quasiparticles on phonons were dropped out. Doing the same kind of calculations as in Section 3.5.1, and keeping just the highest order terms in $A_{s,0}$, $A_{b,0} \equiv \Delta_0/k_B T_b \equiv \beta_b\Delta_0$, and $A_{n,0}$, we obtain the following expressions for the recombination,

$$\Upsilon_{rec}(T_s, x) - \Upsilon_{gen}(T_b, x) = \frac{R n_0^2}{w_s d_s} \frac{\pi\Delta_0}{2} \left[\frac{e^{-2\beta_s(x)\Delta_0}}{\beta_s(x)} - \frac{e^{-2\beta_b\Delta_0}}{\beta_b} \right] , \qquad (3.17)$$

for the density of injected quasiparticles,

$$\int_{\Delta(x)}^{\infty} j_{\mathrm{q}}(U,\epsilon,T_{\mathrm{n}},T_{\mathrm{s}}(x),x)d\epsilon \approx \frac{1}{e^2R_{\mathrm{T}}}\sqrt{\frac{\pi\Delta_0}{2}}\left[\frac{g_{1/2}^{(+)}(a_{\mathrm{n},0})}{\sqrt{\beta_{\mathrm{n}}}} - 2\frac{e^{-\beta_{\mathrm{s}}(x)\Delta_0}}{\sqrt{\beta_{\mathrm{s}}(x)}}\right] \tag{3.18}$$

and for the density of quasiparticle current that tunnels into the trap,

$$\int_{\Delta(x)}^{\infty} j'_{\mathrm{q}}(0,\epsilon,T_{\mathrm{s}},T_{\mathrm{b}},x)d\epsilon \approx \frac{2}{e^2R_{\mathrm{T}}}\sqrt{\frac{\pi\Delta_0}{2}}\left[\frac{e^{-\beta_{\mathrm{b}}\Delta_0}}{\sqrt{\beta_{\mathrm{b}}}} - \frac{e^{-\beta_{\mathrm{s}}(x)\Delta_0}}{\sqrt{\beta_{\mathrm{s}}(x)}}\right]\theta(x-l_{\mathrm{trap}}), \tag{3.19}$$

where θ is the Heaviside function. Since it can be easily checked that the density of injected quasiparticles is much higher than the recombination term, we can neglect the last one in the junction region, and calculate the total current of quasiparticles in the superconductor, at position $x = l$ (see Fig. 3.3). From Eqs. (3.15) and (3.18), this current is:

$$\begin{aligned} J_q(V,T_{\mathrm{n}},T_{\mathrm{s}}(l)) &\approx \frac{1}{e^2R_{\mathrm{T}}}\sqrt{\frac{\pi\Delta_0}{2}}\left[\frac{g_{1/2}^{(+)}(a_{\mathrm{n},0})}{\sqrt{\beta_{\mathrm{n}}}} - 2\frac{e^{-\beta_{\mathrm{s}}(l)\Delta_0}}{\sqrt{\beta_{\mathrm{s}}(l)}}\right] \\ &= -\frac{n_0D_{\mathrm{n}}}{\beta_{\mathrm{s}}(l)}\left.\frac{dy}{dx}\right|_l . \end{aligned} \tag{3.20}$$

Now, if we write

$$\beta_{\mathrm{s}}(x) = -\frac{\log y(x)}{\Delta_0},$$

Eq. (3.15) becomes a second order differential equation for the function $y(x)$, with one boundary condition, at $x = l$, given by Eq. (3.20) and the other one, at $x = \infty$, $y(x=\infty) = e^{-\Delta_0\beta_{\mathrm{b}}}$. Nevertheless, written in this form, the equation has to be integrated numerically. Fortunately we can avoid this situation by noting that, using the properties of inverse functions, we can write

$$\frac{d^2y}{dx^2} = \frac{1}{2}\frac{d}{dy}\left[\left(\frac{dx}{dy}\right)^{-2}\right]. \tag{3.21}$$

Making the notation $y_{\mathrm{f}} \equiv y(\infty) = e^{-\Delta_0\beta_{\mathrm{b}}}$, we can write Eq. (3.15) in the form

$$\begin{aligned} \frac{d}{dy}\left[\left(\frac{dx}{dy}\right)^{-2}\right] &= \frac{Rn_0}{w_{\mathrm{s}}d_{\mathrm{s}}D_{\mathrm{n}}}\pi\Delta_0\left[y^2(x) - y_{\mathrm{f}}^2\frac{-\log[y(x)]}{-\log y_f}\right] \\ &+\frac{4}{e^2R_{\mathrm{T}}}\sqrt{\frac{\pi}{2}}\frac{1}{n_0D_{\mathrm{n}}}\left[y(x)\sqrt{-\log[y(x)]}\right. \\ &\left.-y_{\mathrm{f}}\frac{-\log[y(x)]}{\sqrt{-\log y_f}}\right]\phi(x). \end{aligned} \tag{3.22}$$

Equation (3.22) can be solved using a separation of variable and the boundary conditions given by Eq. (3.20) at $x = l$, and $dy/dx = 0$ at $x = \infty$. In this way we obtain the equation:

$$
\begin{aligned}
\left.\frac{dy}{dx}\right|_l &= \frac{1}{e^2 R_{\mathrm{T}}}\sqrt{\frac{\pi}{2\Delta_0}\frac{-\log[y(l)]}{n_0 D_{\mathrm{n}}}}\left[\frac{g_{1/2}^{(+)}(a_{\mathrm{n},0})}{\sqrt{\beta_{\mathrm{n}}}} - 2y(l)\sqrt{\frac{\Delta_0}{-\log[y(l)]}}\right] \\
&= \left\{\int_{y_{\mathrm{f}}}^{y(l)}\left[\frac{Rn_0}{w_{\mathrm{s}}d_{\mathrm{s}}D_{\mathrm{n}}}\pi\Delta_0\left(y^2 - y_{\mathrm{f}}^2\frac{-\log y}{-\log y_f}\right)\right.\right. \\
&\quad \left.\left. + \frac{4}{e^2 R_{\mathrm{T}}}\sqrt{\frac{\pi}{2}}\frac{1}{n_0 D_{\mathrm{n}}}\left(y\sqrt{-\log y} - y_{\mathrm{f}}\frac{-\log y}{\sqrt{-\log y_f}}\right)\phi\right] dy\right\}^{1/2} .
\end{aligned}
\tag{3.23}
$$

If $l = l_{\mathrm{trap}}$, then $\phi \equiv 1$ in the equation above. If $l \neq l_{\mathrm{trap}}$, Eq. (3.23) has to be splitted in two parts, one for the segment $[l, l_{\mathrm{trap}})$ and the other one for $[l_{\mathrm{trap}}, \infty)$, with the condition that both $y(x)$ and dy/dx are continuous at $x = l$. Equation (3.23) is much easier to solve than the original diffusion equation [Eq. (3.5)] and almost all the integrals can be written in terms of elementary functions.

At low temperatures, solving the coupled equations (3.11) and (3.23), we can obtain directly the cooling performance of the SINIS structure. The conclusions are clear and similar to those obtained from the exact numerical solution: refrigerators do not work at low bath temperature without quasiparticle trap. In the case of small junctions, the trap through the oxide layer is enough to thermalize the superconductor, while in the case of large junctions it is not.

If the gap is not constant, the situation is more complicated since Eq. (3.15) contains terms proportional to $d\Delta(x)/dx$ or $d^2\Delta(x)/dx^2$. One way to apply the same formalism to such a situation is to assume that the gap has jumps at certain positions x_1, $x_2 \ldots$, and solve Eq. (3.22) on intervals, as mentioned before. In any case, this method can be used rather for qualitative than for quantitative evaluations.

Chapter 4

The Core-melted cluster

The study of clusters is important and interesting since the clusters provide a connection between the physics of a few body systems, relatively well known and studied for a long time, and the physics of large, macroscopical objects, which are studied by means of statistical mechanics. This connection was made possible by the advances in computer technology. In this way the motion of the atoms in the cluster and the chemical bonds between them can be simulated, starting from first principles of quantum or classical physics, or statistical ensembles can be constructed, usually by Monte Carlo methods. In this chapter we shall use these techniques to address the problem of phase transitions and to prove the existence of new phases in clusters.

As mentioned in the first chapter, the phases cannot be defined rigorously in small systems. This is due to the fluctuations, which are large compared to the thermodynamical averages. As discussed in Section 1.4 [5], a cluster consisting of a small number of atoms can pass back and forth between different phases. Because of this, in what follows the denomination of phases will be replaced by the more appropriate one of *phase-like forms.*

In this chapter we shall prove the existence of new phase-like forms, like the core-melted and the core-surface-melted phase-like forms. This is done by constructing clusters of atoms that interact by a new type of two-body potential (for more details see Paper V). All the systems under study are classical, and are composed of simple, identical atoms. One feature of the new pair potential introduced in Paper V is that allow the formation of the solid phase which is less dense than the liquid phase. The analytical form of this model potential is

$$V(r) = \begin{cases} \infty & , \; r \in [0, r_0] \\ \epsilon_1 \left(\frac{\sigma_1}{r-r_0}\right)^{12} + V_v - \int_{r_0}^{r} n_1 (x-r_0)^7 & \\ \times (r_1 - x + r_0)^{1/3} \mathrm{d}x & , \; r \in (r_0, r_0 + r_1] \\ 4V_w \left[\left(\frac{\sigma_2}{r-r_0-r_2}\right)^{12} - \left(\frac{\sigma_2}{r-r_0-r_2}\right)^{6} \right] & , \; r \in (r_0 + r_1, \infty) \end{cases} \tag{4.1}$$

which is represented in Fig. 4.1. We shall present briefly the choices we made

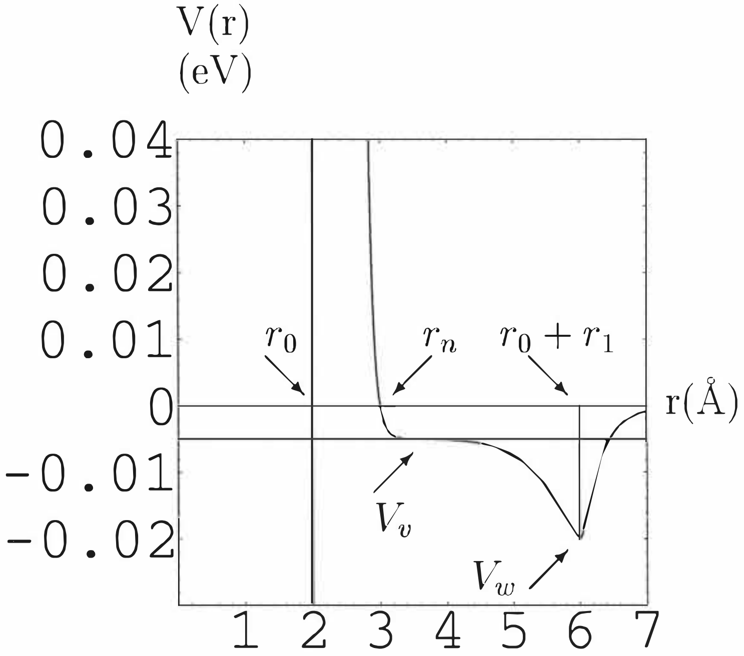

Figure 4.1: Pairwise potential. The potential is 0 at $r = r_n$ and tends to ∞ as $r \to r_0$.

in our simulations for the parameters introduced in Eq. (4.1). We fix from the beginning $\sigma_1 = \sigma_2 = 1$ Å. In the simulations with $V_v < 0$ we choose $\epsilon_1 = -V_v$. For the calculations with $V_v \geq 0$ we used $\epsilon_1 = 0.005$ eV. V_w was always kept equal to -0.02 eV (about double the depth of the potential well used in the case of argon atoms). Once we fix the above mentioned parameters, we calculate n_1 such that $\lim_{r \nearrow r_0 + r_1} V(r) = V_w$ and r_2 such that $\lim_{r \searrow r_0 + r_1} V'(r) = 0$. It is easy to see now that $V \in C^1(r_0, \infty)$. The exponents 7 and 1/3 of $(x - r_0)$ and $(r_1 - x + r_0)$ respectively, in the second branch of Eq. (4.1), can also be changed in order to obtain different widths of the potential well.

The parameters r_0, r_n and V_v (and implicitly n_1) are varied in different simulations to study their influence on the properties of the cluster. We used standard Molecular Dynamics techniques to control the temperature or the energy of the cluster (for details see e.g. [41]).

Because of the deep potential well V_w, the cluster will have an at least local stable solid phase-like form (SP). How well the cluster can reach its minimum potential energy in the solid state, depends on the choice of the other parameters too.

The plateau V_v gives a possibility of the existence of closed packed configurations, which are denser than the solid phase. The stability of this phase is assured, not by the nearest neighbour interaction, but by the interaction of distant atoms. The nearest neighbours will interact just repulsively, in some cases very strongly. The atoms are pushed together by atoms further out. Let us imagine that we have a macroscopical quantity of such a phase between two slabs (the liquid should wet the slabs) and measure the shear viscosity. Due to the length of the plateau, the atoms can be viewed as moving in an average potential and have collisions with the nearest neighbours. In this case, the shear viscosity is expected to be lower than in the SP, where the atoms are fixed in their positions by nearest neighbour interactions. Consequently we can say that we have a "dense liquid" phase (DLP), but we could have also called it a glass phase, since, especially at low temperatures, the atoms do not exhibit diffusive motion and the cluster is usually more disordered than in the solid phase. Depending mainly on the ratio of r_0 and r_1 and on V_w and V_v, this phase-like form could be more stable or less stable than the solid phase-like form. The core-melted cluster (CMC) can be formed in both situations, but it appears to be more natural in the case when the solid is more stable than the dense liquid. For each fixed r_1, V_w and V_v there will be an r_0 at which the stability will change. At low r_0 the liquid phase is more stable.

The denomination "core-melted cluster" is justified by the following facts: (1) The nearest neighbour distance of the atoms in the outer shell of atoms is close to $r_0 + r_1$, as in the case of SP, while the nearest neighbour distance between the atoms in the core is much smaller. (2) Measuring the mean square displacement of the atoms in the outer shell and in the core, we obtain large differences (up to two orders of magnitude or more, depending, of course, on the temperature). For some choices of parameters we can observe a clear diffusive motion of the atoms in the core.

At higher temperatures (higher than the temperatures at which the two phases, DLP and CMC, mentioned above are stable) we see another "liquid" phase (LP), which is much more disordered and less dense than the DLP. The qualitative difference between these two phases appear more obvious at larger r_0, and especially in the region where the energy of the solid state is lower than that of the DLP. In the LP, the minimum distance at which two neighbouring atoms can get is larger than in the DLP. Usually, for normal substances, this distance is decreasing with increase of temperature (as long as the liquid or the solid phase is preserved), due to the increase of the kinetic energy. When the cluster is in the liquid phase-like form, the surface atoms are evaporating.

In any situation the transition from the CMC to the liquid cluster (LC) is made through the core-surface-melted cluster. This means that before the transition to the liquid phase-like form, the atoms belonging to the external shell of the core-melted cluster become *floaters* (see [5] for the definition). In this respect the transition is very similar to the transition from the solid phase-like form to

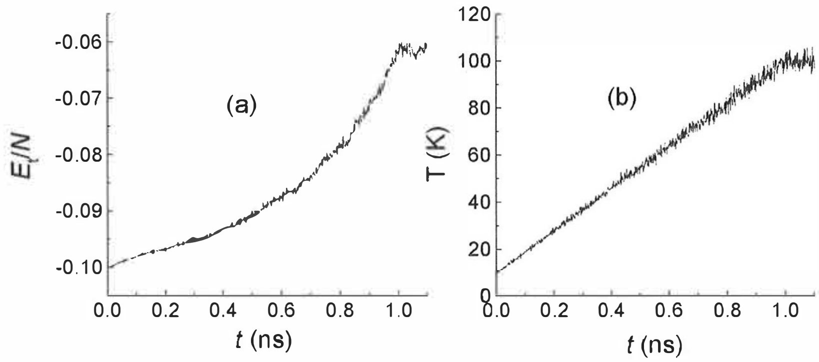

Figure 4.2: The total energy divided by the number of atoms, E_t/N, **(a)** and the temperature of the cluster, T, **(b)** vs. time, for an icosahedral cluster in DLP, with $r_0 \approx 3.7$ Å.

liquid phase-like form.

As described in Paper V, for the chosen set of parameters – $r_1 = 4$ Å, $V_v = -0.005$ eV and $V_w = -0.02$ eV (the other parameters are: $\sigma_1 = \sigma_2 = 1$ Å, $\epsilon_1 = 0.005$ eV, $r_2 \approx 2.88$ Å, and $n_1 = 1.31989 \times 10^{-8}$) – at low r_0 the DLP is more stable than the SP. In the calculations it turned out that the stability changes at $r_0 \approx 4$ Å, but this depends on the choice of the other parameters too, especially on V_v and V_w. Therefore, the clusters that after the equilibration were in the DLP will stay like that until they start to evaporate. As mentioned before, in this phase-like form, at low temperatures, the atoms have low mobility (comparable to the mobility in the solid phase). As the temperature increases, the mobility increases and, gradually, the atoms start to have diffusive motion, or evaporate. The transition between these two regimes is much smoother than, for example solid-liquid transition, and resembles more to a *glass transition*. As an example we show in Fig. 4.2 the total energy of a cluster, devided by the number of atoms, as the temperature increases from 10 to 100 K. The cluster consists of 923 atoms and it was equilibrated at 10 K in a DLP icosahedral configuration. The parameter r_0 was choosen to be about 3.7 Å. We can observe in this figure the gradual bending upwards of the (average) total energy curve, at the onset of the diffusive atomic motion. In these cases the DLP and LP could be considered to be the same. The CMC and SP clusters are unstable and collapse to DLP (see Fig. 4.3).

For higher r_0 ($r_0 > 4$ Å) the SP is more stable than the DLP. The CMC is still collapsing, but to the LP, at basically the same melting temperature as the solid type of clusters. Moreover, there is a critical r_0 (in our calculations is 6

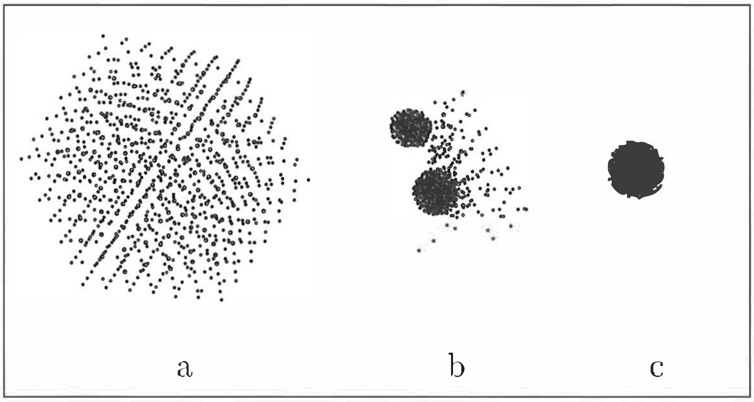

Figure 4.3: $r_0 = 0$. a) core-melted cluster; b) collapsing to dense-liquid cluser; c) dense-liquid cluster.

Å) above which the icosahedral DLC transform into CMC at lower and lower temperatures, as r_0 increases. This case is presented in Fig. 4.4.

To illustrate the properties of the CMC mentioned above, we show in Fig. 4.5 a), b) the average nearest neighbour distance and the maximum mean square displacement for each shell in an icosahedral core-melted cluster with 923 atoms and with $r_0 = 4.2$ Å. Of course, there exists a mixing between the inner shells. It should also be noted that the diffusion of the core atoms is limited by the solid shell and by the fact that they have quite big dimensions (we could say that the radius of the atom is about r_n). Modifying the parameters of the potential one can change the mobility of the core atoms and the stability of the solid phase (or of the solid shell). As an example, we plotted in Fig. 4.5 (c) the maximum mean square displacement for each shell of an icosahedral core-surface melted cluster ($N = 1415$ atoms, $r_0 = 3.7$ Å, $-V_v = \epsilon_1 = 0.002$ eV, $V_w = -0.02$ eV and $n_1 = 1.58386 \times 10^{-8}$, the rest of the parameters being the same as before). In the same figure ((d) and (e)) are shown the mean square displacement vs time of the atoms in the shells 1 and 7, to emphasize the diffusive motion. The simulation is carried on at constant energy, with the average kinetic energy corresponding to a temperature of 60 K. It can be seen that the outermost shell is not stable and some diffusive motion over the surface is present. This case would get into the category of the core-surface-melted clusters. Bigger displacements of the core or surface atoms can be obtained by increasing the temperature. Anyway, in these cases the cluster might stay in this state for a shorter time.

An interesting note is that, even when $V_v = 0$ the cluster can be found in all the above mentioned phase-like forms. There exists a value $V_v > 0$ above which the DLP and CMC disappear.

Starting from an icosahedral configuration one can never achieve, with this kind of interaction potential, a SP cluster. The strain between the atoms in the

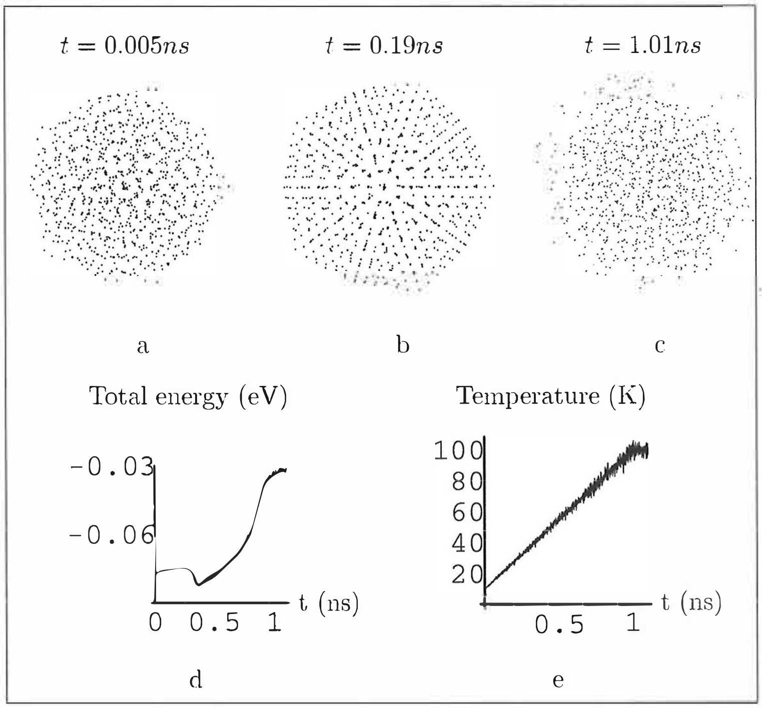

Figure 4.4: $r_0 = 6.9$ Å. Transition from dense-liquid cluster to liquid cluster, through core-melted cluster, as the temperature increases.

shells [42] contract the surface into the solid phase and make the core collapse to the liquid phase. This was observed in all the simulations. On the other hand we never observed a CMC with the external structure of a Wulff polyhedron. This kind of polyhedron is based on an fcc lattice, hence, if the distance between the atoms in the (111) planes is about $r_0 + r_1$, then the nearest neighbour distance in the (100) plane is about $\sqrt{2}(r_0 + r_1)$. Since in this kind of potential $r_0 + r_1$ is much bigger than the half width of the deep potential well, the binding between the atoms in the last case is negligible. Therefore the atoms in the (100) facets will not reach a solid configuration. Fortunately for the existence of the CMC, in the formation of clusters the structures with closed packed atoms on the surface are preferred, since these have a smaller surface energy.

In conclusion, introducing a new type of pair interaction we were able to obtain a phase-like form of clusters (the core-melted clusters) in which the shell is solid, while the core atoms are very mobile. For a proper choice of the parameters of the potential, at a certain temperature range, we can observe diffusive motion of the inside atoms. In addition, another new phase was found: the core-surface-melted phase.

The atoms interacting with this type of potential can have, beside the "pure" solid and liquid phases, another phase, which we call the *dense liquid* phase.

When cooling down the cluster from the liquid phase the cluster will solidify with difficulty. Usually, in the case that the solid phase is more stable than the dense liquid, the cluster will stay super-cooled for long time.

The stability of the different phases depends mainly on the ratios of the parameters, such as $r_0/(r_0+r_1)$ and V_v/V_w. Of course, the dynamics of the atoms in the cluster is changing when modifying the parameters, but the potential energy of different configurations or the relative potential energies, which determine the stability of the phase-like forms, depend in principle on these quantities.

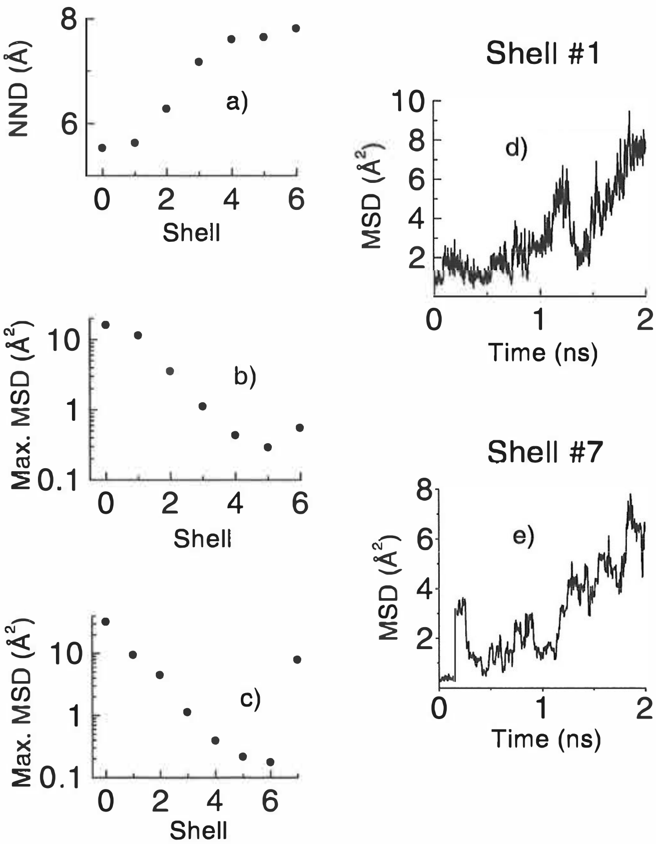

Figure 4.5: In figures (a) and (b) we plot the average nearest neighbour distance (NND) and, respectively, the maximum mean square displacement (Max. MSD) in each shell for an icosahedral core-melted cluster consisting of 923 atoms ($V_v = -0.005$ and $V_w = -0.02$ eV). For an icosahedral core-surface-melted cluster, consisting of 1415 atoms, we show the maximum mean square displacement in each shell (c), the mean square displacement vs time in shell 1 (d) and in shell 7 (e) ($V_v = -0.002$ eV and $V_w = -0.02$ eV). Both clusters were simulated for 2 ns.

Chapter 5

Summary

After a general introduction to the physics of phase transitions in Chapter 1, the heat conduction by phonons in ultrathin membranes was analyzed in Section 2.1.1. Taking explicitly into account the finite width of the membrane, we observed a cross-over from a bulk three dimensional phonon distribution to a quasi two dimensional one when the temperature is lowered. The corresponding changes in the relevant thermodynamic quantities were calculated and the results were compared with the experimental data (Paper I and Paper II).

Due to the analogies with the multiple-step Bose-Einstein condensation [12, 13], the change in the dimensionality of the particle distribution was called Bose-like condensation. The extension of this concept from the case of the phonon gas to the systems of massive particles was done in Paper III, which is reviewed in Section 2.1.2 of this thesis. In the low density limit, the Bose-like condensation is similar for both types of particles and, for some energy spectra, exhibits features specific to multiple-step Bose-Einstein condensation, for instance the appearance of maxima in the specific heat.

In the case of fermions, another phenomenon was observed. For certain types of single particle hamiltonians, the specific heat is asymptotically approaching a divergent behavior at zero temperature, as the Fermi energy ϵ_{F} is converging towards any value from an infinite discrete set of energies: $\{\epsilon_i\}_{i\geq 1}$. The divergent behavior for $\epsilon_{\mathrm{F}} = \epsilon_i$, for any i, is specific only to infinite systems. If the system is finite, the specific heat converges to zero at zero temperature, for any ϵ_{F}, as expected. All the results are particularized for particles trapped inside parallelepipedic boxes and harmonic potentials.

The diffusion of nonequilibrium quasiparticles in a superconductor was investigated in Chapter 3 [Paper IV]. It was shown that if a normal metal trap is attached to the superconducting wire, through an insulating oxide layer or in direct metal-to-metal contact, the thermalisation of the superconductor is much faster. In the first case this is due to the tunneling of the excess quasiparticles into the normal metal trap, and in the second case due to the nonuniform energy gap induced into the superconductor by the normal metal. These theoretical results explained the experimental observations and helped improve the design of refrigerators based on normal metal-insulator-superconductor tunnel junctions.

In Chapter 4, a new phase-like form of clusters is presented, namely the *core-melted cluster.* With a new type of interaction potential (see Fig. 4.1), we were able to construct a cluster with a shell consisting of atoms which are vibrating around regular crystalline sites, while the core atoms have much bigger mobility and sometimes exhibit a diffusive motion. In addition to the core-melted phase, the dense-liquid phase and the core-surface-melted phase were found (see Paper V).

Bibliography

[1] K. Huang, *Statistical Mechanics*, 2nd ed., Wiley, New York (1987).

[2] H. B. Callen, *Thermodynamics, an introduction to the physical theories of equilibrium thermostatistics and irreversible thermodynamics*, John Wiley & Sons, Inc., New York (1985).

[3] A. L. Fetter and J. D. Walecka, Quantum theory of many particle systems, McGraw-Hill, Inc., New York (1971).

[4] C. N. Yang and T. D. Lee, Phys. Rev. **87**, 404 (1952); T. D. Lee and C. N. Yang, Phys. Rev. **87**, 410 (1952)

[5] R. Stephen Berry, *Phases and Phase Changes of Clusters*, in Large Clusters of Atoms and Molecules, pp 281–295, ed. by T. P. Martin (Kluwer, Dordrecht, The Netherlands, 1996).

[6] R.M. Ziff, G.E. Uhlenbeck, and M. Kac, Phys. Rep. **32**, 169 (1977).

[7] V. Bagnato, D. E. Pritchard, and D. Kleppner, Phys. Rev. A **35**, 4354 (1987).

[8] V. Bagnato and D. Kleppner, Phys. Rev. A **44**, 7439 (1991).

[9] M. H. Anderson, J. R. Ensher, M. R. Matthews, C. E. Wieman, and E. A. Cornell, Science **269**, 198 (1995); C. C. Bardley, C. A. Sackett, J. J. Tollet, and R. G. Hulet, Phys. Rev. Lett. **75**, 1687 (1995); K. B. Davis, M.-O. Mewes, M. R. Andrews, N. J. van Druten, D. S. Durfee, D. M. Kurn, and W. Ketterle, Phys. Rev. Lett. **75** 2909 (1995).

[10] S. Grossmann and M. Holthaus, Phys. Lett. A **208**, 188 (1995).

[11] L. N. Cooper, Phys. Rev. **104** 1189 (1956).

[12] E. B. Sonin, Sov. Phys. JETP **29**, 520 (1969).

[13] N. J. van Druten and W. Ketterle, Phys. Rev. Lett. **79**, 549 (1997).

[14] M. H. Lee, J. Math. Phys. **36**, 1217 (1995).

[15] W. Ketterle and N. J. van Druten, Phys. Rev. A **56**, 656 (1996)

[16] D. F. Goble and L. E. H. Trainor, Can. J. Phys. **44**, 27 (1965).

[17] D. F. Goble and L. E. H. Trainor, Phys. Rev. **157**, 167 (1967).

[18] D. A. Krueger, Phys. Rev. Lett. **19**, 563 (1967); Phys. Rev. **172**, 211 (1968).

[19] R. K. Pathria, Phys. Rev. A **5**, 1451 (1972).

[20] S. Greenspoon and R. K. Pathria, Phys. Rev. A **8**, 2657 (1973);

[21] S. Greenspoon and R. K. Pathria, Phys. Rev. A **9**, 2105 (1974);

[22] S. Greenspoon and R. K. Pathria, Phys. Rev. A **11**, 1080 (1975).

[23] Paper V of this thesis.

[24] M.M. Leivo and J.P. Pekola, Appl. Phys. Lett. **72**, 1305 (1998).

[25] J. P. Pekola, A. J. Manninen, M.M. Leivo, K. Arutyunov, J.K. Suoknuuti, T.I. Suppula, and B. Collaudin, to be published in Physica B (2000).

[26] J.M. Ziman, *Electrons and Phonons: The Theory of Transport Phenomena in Solids*, Oxford University Press (1979).

[27] W. Holmes, J.M. Gildemeister, P.L. Richards and V. Kotsubo, Appl. Phys. Lett. **72**, 2250 (1998).

[28] M. Apostol, Phys. Rev. E **56**, 4854 (1997).

[29] F. C. Wellstood, C. Urbina, and J. Clarke, Phys. Rev. B **49**, 5942 (1994).

[30] M. Tinkham, *Introduction to superconductivity*, Second Ed., McGraw-Hill, Inc. (1996).

[31] B. D. Josephson, Phys. Lett. **1**, 251 (1962).

[32] J. Bardeen, Phys. Rev. Lett. **9**, 147 (1962).

[33] J. Jochum, C. Mears, S. Golwala, B. Sadoulet, J. P. Castle, M. F. Cunningham, O. B. Drury, M. Frank, S. E. Labov, F. P. Lipschultz, H. Netel, B. Neuhauser, J. Appl. Phys. **83**, 3217 (1998).

[34] S. Guéron, H. Pothier, N. O. Birge, D. Esteve, and M. H. Devoret, Phys. Rev. Lett. **79**, 3490 (1997)

[35] C. J. Pethick and D. Pines, Phys. Rev. Lett. **57**, 118 (1986).

[36] J. N. Ullom, P. A. Fisher, and M. Nahum, Phys. Rev. B **58**, 8225 (1998).

[37] J. Bardeen, L. N. Cooper, and J. R. Schrieffer, Phys. Rev. **108**, 1175 (1957).

[38] M.M. Leivo, J.P. Pekola, and D.V. Averin, Appl. Phys. Lett. **68**, 1996 (1996).

[39] J. P. Pekola et. al., unpublished.

[40] A. Bardas and D. Averin, Phys. Rev. B **52**, 12873 (1995).

[41] M. P. Allen, D. J. Tildesley, Computer simulations of liquids, Oxford University Press, New York, 1990.

[42] T. P. Martin, Phys. Rep. **273**, 199 (1996).